ChemComm

FEATURE ARTICLE

Cite this: *Chem. Commun.*, 2023, **59**, 2541

Zr- and Ti-based metal–organic frameworks: synthesis, structures and catalytic applications

Ji Li,[ab] Jin-Yi Huang,[a] Yu-Xuan Meng,[a] Luyan Li,[d] Liang-Liang Zhang *[abc] and Hai-Long Jiang *[d]

Received 21st December 2022,
Accepted 17th January 2023

DOI: 10.1039/d2cc06948b

rsc.li/chemcomm

Recently, Zr- and Ti-based metal–organic frameworks (MOFs) have gathered increasing interest in the field of chemistry and materials science, not only for their ordered porous structure, large surface area, and high thermal and chemical stability, but also for their various potential applications. Particularly, the unique features of Zr- and Ti-based MOFs enable them to be a highly versatile platform for catalysis. Although much effort has been devoted to developing Zr- and Ti-based MOF materials, they still suffer from difficulties in targeted synthesis, especially for Ti-based MOFs. In this Feature Article, we discuss the evolution of Zr- and Ti-based MOFs, giving a brief overview of their synthesis and structures. Furthermore, the catalytic uses of Zr- and Ti-based MOF materials in the previous 3–5 years have been highlighted. Finally, perspectives on the Zr- and Ti-based MOF materials are also proposed. This work provides in-depth insight into the advances in Zr- and Ti-based MOFs and boosts their catalytic applications.

1 Introduction

MOFs are assembled from the combination of a cation/cluster and a negatively charged organic linker bearing a complexing function. The diversity in the selection of organic and inorganic components, together with the crystalline, porous and tailorable nature, allows for a variety of MOFs with adjustable surface area, pore environment and functionality. As a class of emerging porous network materials, MOFs exhibit potential applications, including gas adsorption and separation, sensing, heterogeneous catalysis, magnetism and drug delivery.[1–7] However, the early

[a] *Strait Laboratory of Flexible Electronics (SLoFE), Strait Institute of Flexible Electronics (SIFE, FutureTechnologies), Fujian Normal University, Fuzhou 350117, Fujian, P. R. China. E-mail: ifellzhang@fjnu.edu.cn*
[b] *Institute of Flexible Electronics, Northwestern Polytechnical University, Xi'an 710072, ShaanXi, P. R. China*
[c] *Ningbo Institute of Northwestern Polytechnical University, Ningbo 315103, Zhejiang, P. R. China*
[d] *Department of Chemistry, University of Science and Technology of China, Hefei, Anhui 230026, P. R. China. E-mail: jianglab@ustc.edu.cn; Web: https://mof.ustc.edu.cn/*

Ji Li

Ji Li obtained her Bachelor's Degree in Material Physics from Southwest University in 2021. After that, she pursued her master's degree in chemistry under the supervision of Professor Liangliang Zhang at Northwestern Polytechnical University. Her research interests are functional Zr- and Ti-based MOFs and their applications.

Liang-Liang Zhang

Liangliang Zhang received his PhD in Inorganic Chemistry from Shandong University under the supervision of Prof. Daofeng Sun. In 2013, he joined the faculty of China University of petroleum. He worked in Prof. Hongcai Zhou's group at Texas A&M University as a visiting scholar during 2016-2017; then, he moved to Northwestern Polytechnical University in 2018. He worked with Prof. Hai-Long Jiang at USTC for a while in 2019. Currently, he works in Fujian Normal University. His research interests are centered on the construction of high-valence porous MOFs and their catalytic applications.

MOFs suffer from moisture sensitivity, which limits their use in real applications. One of the most effective methods to overcome this problem is coating a hydrophobic reagent on the surface of MOFs, such as polydimethysiloxane (PDMS).[8] Another powerful strategy is using high valent metal ions to enhance the strength of the coordination bond and the chemical stability.

As an important branch, MOFs based on carboxylate and high valent Zr^{IV} and Ti^{IV} metal ions have been of particular interest, since the first discoveries of UiO-669 and MIL-125.[10] According to the principle of reticular chemistry, a large set of Zr- and Ti-based MOFs have been synthesized rationally based on the versatile connectivity of Zirconium and Titanium clusters and the capable tunability of organic ligands.[4] Although great efforts have been made in the past few decades, how to precisely control the efficient preparation of targeted MOFs is still a challenge. Compared with Zr-MOFs, Ti-MOFs are in their infancy, although Ti-MOFs possess unique photochemical activity. The further development of Zr- and Ti-based MOFs is closely related to their intrinsic properties of highly charged cations.

The focus of this feature article is on the history and advancement of Zr- and Ti-based MOFs based on carboxylate. First of all, the nature of zirconium and titanium cations and clusters is discussed, which is helpful for understanding the chemical reactivity in the solution. Then, the synthesis and structures of representative Zr- and Ti-based MOFs are presented in terms of different Zr- and Ti-based secondary building units and organic ligands. Moreover, we also talk about the multivariate MOFs (MTV-MOFs) and Zr- and Ti-based MOF composites and derivatives because of the construction of a collaborative catalysis system. Thus, we highlight the catalytic applications of Zr- and Ti-based MOF materials, including pristine MOFs and MOF composites and derivatives. Finally, we provide perspectives on the Zr- and Ti-based MOFs (Scheme 1).

Hai-Long Jiang

Hai-Long Jiang earned his PhD (2008) in Inorganic Chemistry from Fujian Institute of Research on the Structure of Matter, Chinese Academy of Sciences. He subsequently worked at the National Institute of Advanced Industrial Science and Technology (AIST, Japan), first as an AIST Fellow and later as a JSPS Fellow during 2008-2011. After a postdoctoral stint at Texas A&M University (USA), he became a full professor at USTC in 2013. He was elected a Fellow of the Royal Society of Chemistry (FRSC) in 2018 and has been annually listed as a highly cited researcher (chemistry) by Clarivate Analytics since 2017. His research interest currently lies in biomimetic microenvironment modulation (MEM) of catalytic centers based on crystalline porous materials (particularly MOFs).

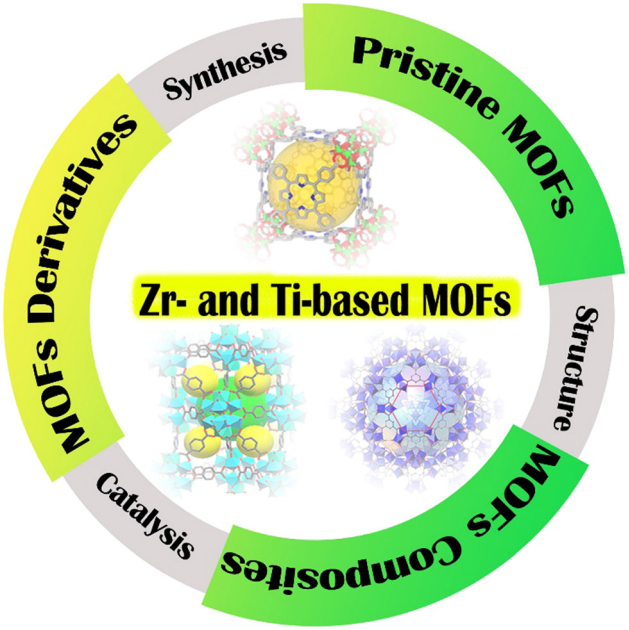

Scheme 1 Schematic illustration of the synthesis, structures and catalytic applications of Zr- and Ti-based MOFs.

2 The chemistry of zirconium and titanium cations and clusters

As an important component of Zr- and Ti-based MOFs, the physicochemical properties of the high valent cation have to be considered in order to deeply understand the essence of the chemical reactivity of the various cations, including the charge, size, electronegativity and so on. The charges of both Zr and Ti are in the +4 oxidation state and they are in the same Group IV in the periodic table. However, the ionic radius, electronic configuration and coordination asymmetry of Ti^{4+} and Zr^{4+} are different, leading to large differences in physical properties and coordination topologies. In fact, the combination of ionic radius and charge plays an important role in coordinating with organic linkers in aqueous solution.[11] According to the Pourbaix diagrams of Ti in water, it should also be pointed out that the oxides or hydroxides of Ti dominate a large range of pH area even under quite acidic conditions.[12] That's why Ti-MOFs are often yielded under an environment of excess acid to avoid the formation of oxide or hydroxide species.

Considering the high activities of high valent Zr^{IV} and Ti^{IV} metal ions, Zr-oxo-clusters and Ti-oxo-clusters are usually applied to build up extended coordination compounds as precursors. As shown in Fig. 1, in Zr-MOFs, there are diverse clusters observed in cluster chemistry, such as Zr_3, Zr_4, Zr_5, Zr_6, Zr_8, Zr_{10}, Zr_{12}, Zr_{18} and Zr_{36} clusters, but the dominating cluster is Zr_6 clusters with varying connectivity.[13–16] For the Ti-oxo clusters, numbers of Ti atoms in Ti-oxo clusters vary from 3 to 32 and the carboxylate based Ti-oxo-clusters can range from 3 to 10, such as Ti_3, Ti_4, Ti_6, Ti_8, and Ti_9.[17] The excellent tolerance towards defects guarantees Zr-oxo-clusters extremely fast progress, including the easy development of isoreticular structures and the

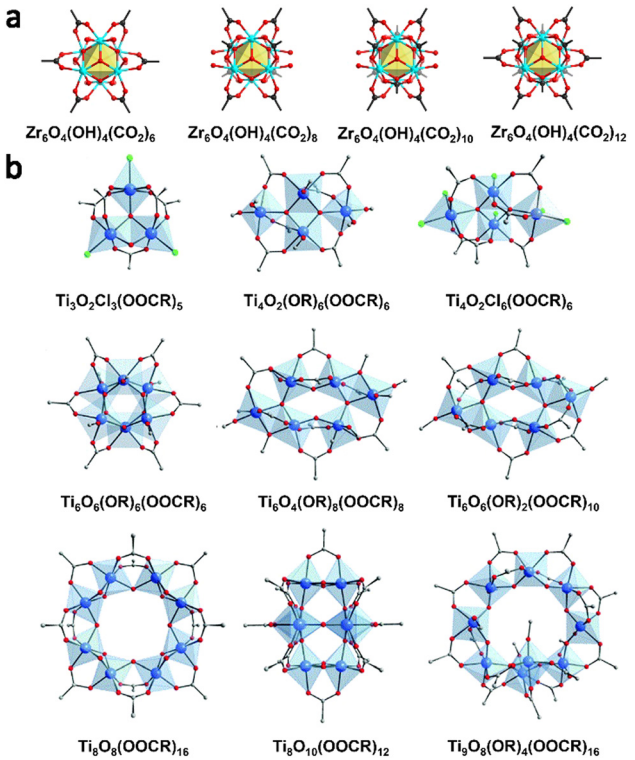

Fig. 1 Selected (a) Zr and (b) Ti-oxo-carboxylate clusters. Reproduced from ref. 17 with permission from the Royal Society of Chemistry, copyright 2017.

possibility of using modulators. The Ti-oxo-clusters often suffer from being completely transformed during the reaction, which makes it difficult to predict the structures and hinder the applications. So, a versatile synthetic and theoretical route for the preparation of Ti-MOFs is urgently needed.

2.1 The development of Zirconium MOFs

Researchers have been dedicated to the development of Zr_6-based MOFs since the first zirconium(IV)-carboxylate MOF (Zr-MOF), UiO-66, was solvothermally synthesized by combining $ZrCl_4$ with 1,4-benzenedicarboxylic acid (H_2BDC) in 2008,[9] owing to their superior chemical and thermal stability and tunable connectivity. The hexanuclear Zr cluster is the key factor for the stabilization of the framework. Afterwards researchers obtained lots of stable Zr-MOFs consisting of a Zr_6 cluster (such as PCN-222–225, MOF-525–545, MMPF-6 and NU-1000). In this section, Zr_6 cluster-based MOFs will be discussed in detail according to the topology by the combination of different linkers and Zr_6 clusters, such as (2,12), (3,6), (3,8), (3,12), (4,8), and (4,12)-connected MOFs (Fig. 2). Besides, the symmetry and geometry of linkers and clusters have also been taken into consideration from the view point of topology (Table 1).

2.1.1 Zr-MOFs based on ditopic carboxylic ligands. Since the discovery of UiO-66, various isoreticular MOFs with the same (2,12)-connected **fcu** topology have been documented. Linear dicarboxylate ligands with varying lengths and functional groups have also been designed and explored, which has given rise to tremendous advances in the field of Zr-MOFs.[18,19] However, the window size of a (2,12)-connected **fcu** net limits the accessibility of pore shape and size. Additionally, longer linear linkers may lead to interpenetration, undesired topologies and the blockage of pores.[20,21] Efforts have been made to resolve these issues, such as stepwise ligand exchange, sequential linker labilization and reinstallation[22] and continuous variation of the lattice metric in mixed-linker MOFs.[23]

Another domain topology for ditopic carboxylate and Zr_6 cluster is (2,8)-connected net employing bent or twisted ligands. For example, DUT-51 was synthesized in a solvothermal reaction based on bent DTTDC ligands and an 8-connected octahedral Zr_6 cluster with **reo** topology.[24] A similar situation can also be found in DUT-67.[25] Thus, the use of a twisted ligand with steric hindrance gives rise to PCN-700 with **bcu** topology. In the structure of PCN-700, the Zr_6 cluster is 8 connected and the left uncoordinated OH^-/H_2O group can be further decorated by functional ditopic linkers yielding multicomponent MOFs.[26,27] The pore environment and functionality are precisely modulated by linker installation. Thus, 10-connected and 11-connected Zr_6 clusters can also be realized from their parent 8-connected octahedral Zr_6 cluster after sequential linker installation. The first uninodal 10-connected Zr-MOF with **bct** topology was prepared by regulation of acetic acid amount during the synthesis. There are octahedral cages and channels in the structure of DUT-69.[25] When the bending angle equals 90°, a one-dimensional DUT-80 chain can be obtained with 8-c Zr clusters and cdc ligands.[28] Interestingly, the assembly of V-shaped dicarboxylic acid with Zr_6 clusters can also result in a two-dimensional zirconium based coordination polymer, named LMOF-601. The Zr_6 node, coordinated with 8 SDBA ligands, can be viewed as the 4-c node and the topology of LMOF-601 is **sql** topology.[29] Recently, Yin demonstrated a Zr-PDI MOF based on *N*,*N*′-di-(4-benzoic acid)-1,2,6,7-tetrachloroperylene-3,4,9,10-tetracarboxylic acid diimide ligand and $Zr_6(\mu_3\text{-}O)_4(\mu_3\text{-}OH)_4$ clusters. In Zr-PDI, P-2COOH adopts 8 connected with a dihedral angle of 38.3°, due to the electrostatic repulsion and steric hindrance of the chloro element.[30] The connectivity of Zr_6 clusters can be further reduced to 6. For example, Kaskel confirmed the connectivity of the cluster could switch from 12(DUT-52) to 8(DUT-53) and 6(DUT-84). The structure of DUT-84 belongs to a 6-connected (4,4) **IIb** net with a 2D structure.[31] In addition to linear ligands, some bent ligands have also been investigated to build Zr-MOFs. Recently, diverse MOFs with a geometry mismatch have been intensively reviewed.[32]

2.1.2 Zr-MOFs based on tritopic carboxylic ligands. Yaghi reported the first Zr-MOF, denoted as MOF-808, by using tritopic H_3BTC ligands. MOF-808 crystallizes in the space group of $Fd\bar{3}m$. Each $Zr_6O_4(OH)_4(CO_2)_6$ cluster is connected to six BTC^{3-} ligands and each BTC^{3-} ligand is coordinated to three SBUs giving rise to a (3,6)-connected 3D microporous framework with **spn** topology.[33] Then, Zhou *et al.* synthesized PCN-777 by isoreticular expansion, in which trigonal-planar TATB ligands coordinate with six-connected D_{3d}-symmetric Zr_6 clusters of antiprismatic configuration to form super-tetrahedra as the face. However, the pore size of zeotype PCN-777 with a β-cristobalite-

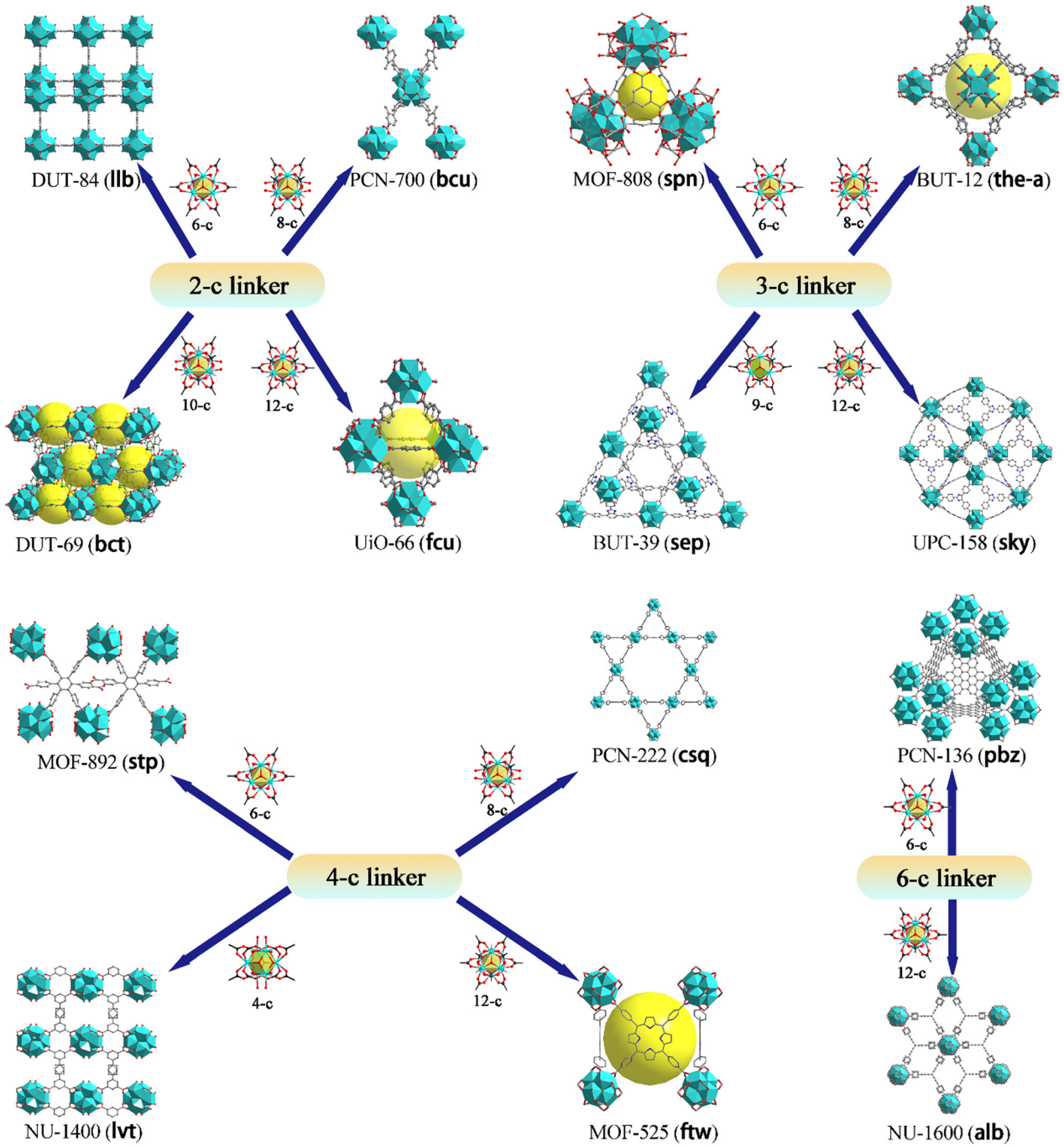

Fig. 2 Representative Zr-MOFs with 12-, 10-, 9-, 8-, 6- and 4-connected Zr_6 clusters and organic linkers. DUT-84[31] (**llb**) consists of 6-c Zr_6 clusters and ditopic linkers; PCN-700[26] (**bcu**) is made from 8-c Zr_6 clusters and 2-c linkers; DUT-69[25] (**bct**) is generated from 10-c Zr_6 clusters and 2-c H_2TDC linkers; UiO-66[9] (**fcu**) is synthesized from 12-c Zr_6 clusters and linear 2-c linkers; MOF-808[33] (**spn**), BUT-12[37] (**the-a**), BUT-39[40] (**sep**) and UPC-158[44] (**sky**) are formed by 6-c, 8-c, 9-c and 12-c Zr_6 clusters and 3-c linkers, respectively; the 4-c linkers join different 4-c, 6-c, 8-c and 12-c Zr_6 clusters to form NU-1400[64] (**lvt**), MOF-892[65] (**stp**), PCN-222[46] (**csq**), MOF-525[45] (**ftw**), respectively; PCN-136[73] (**pbz**) and NU-1600[74] (**alb**) are made from 6-c linkers and different Zr_6 clusters.

type structure reaches up to the mesoporous range, due to the larger size of the TATB linker.[34] Using a non-coplanar H_3BTB ligand, our group has succeeded in preparing the first Zr-BTB MOF with a 2D → 3D interpenetration structure. Each set of Zr-MOF belongs to (3,6)-connected **kgd** topology. In the structure of Zr-BTB, the hexagon $Zr_6O_4(OH)_4(CO_2)_6$ cluster was connected by six carboxylate groups from six BTB ligands and each BTB ligand was connected by three $Zr_6O_4(OH)_4(CO_2)_6$ clusters.[35] After that, Lin and Wang synthesized a series of two-dimensional metal–organic Layers based on tritopic carboxylic ligands.[36]

To further increase the twist angle of tritopic ligands, Li and co-workers reported the first (3,8)-connected Zr-MOF with **the-a**

Table 1 Representative Zr-MOFs based on carboxylic ligands

Zr-MOF	Organic linker	Zr cluster	Topology	Ref.
UiO-66	1,4-Benzenedicarboxylic acid (H_2BDC)	$Zr_6O_4(OH)_4$	(2,12)-Connected **fcu**	9
DUT-51	Dithieno[3,2-*b*;2′,3′-*d*]-thiophene-2,6-dicarboxylate (DTTDC)	$Zr_6O_6(OH)_2$	(2,8)-Connected **reo**	24
PCN-700	2,2′-Dimethylbiphenyl-4,4′-dicarboxylate (Me_2-BPDC)	$Zr_6O_4(OH)_8(H_2O)_4$	(2,8)-Connected **bcu**	26
DUT-69	2,5-Thiophenedicarboxylic acid (H_2TDC)	$Zr_6O_4(OH)_4(H_2O)_2$	(2,10)-Connected **bct**	25
DUT-80	9*H*-Carbazole-3,6-dicarboxylate (CDC)	$Zr_6O_4(OH)_4$	One-dimensional chain	28
LMOF-601	4,4′-Sulfonyldibenzoate (sdba)	$Zr_6O_4(OH)_4$	Two-dimensional **sql**	29
Zr-PDI	*N*,*N*′-Di-(4-benzoicacid)-1,2,6,7-tetrachloroperylene-3,4,9,10-tetracarboxylic acid diimide (P-2COOH)	$Zr_6O_4(OH)_4$	(2,8)-Connected **dia**	30
DUT-84	2,6-Naphthalenedicarboxylate (2,6-ndc)	Zr_6O_8	(2,6)-Connected (4,4) IIb	31
MOF-808	1,3,5-Benzenetricarboxylic acid (H_3BTC)	$Zr_6O_4(OH)_4$	(3,6)-Connected **spn**	33
PCN-777	4,4′,4″-*s*-Triazine-2,4,6-triyl-tribenzoate (TATB)	$Zr_6O_4(OH)_{10}(H_2O)_6$	(3,6)-Connected **spn**	34
Zr-BTB	5′-(4-Carboxyphenyl)-[1,1′:3′,1″-terphenyl]-4,4″-dicarboxylic acid (H_3BTB)	$Zr_6O_4(OH)_4$	(3,6)-Connected **kgd**	35
BUT-12	5′-(4-Carboxy-phenyl)-2′,4′,6′-trimethyl-[1,1′:3′,1″-terphenyl]-(4,4″-dicarboxylic acid) (H_3CTTA)	$Zr_6O_4(OH)_8(H_2O)_4$	(3,8)-Connected **the-a**	37
BUT-13	6,6′,6″-(2,4,6-Trimethylbenzene-1,3,5-triyl) tris (2-naphthoic acid) (H_3TTNA)	$Zr_6O_4(OH)_8(H_2O)_4$	(3,8)-Connected **the-a**	37
BUT-39	4,4′,4″-(1*H*-Benzo[*d*]imidazole-2,4,7-triyl) tribenzoic acid (H_3BTBA)	$Zr_6O_4(OH)_7(H_2O)_3$	(3,9)-Connected **sep**	40
Corrole-MOF-1	(5,10,15-Tris(*p*-Carboxylphenyl)corrole) (H_3TCPC)	$Zr_6O_4(OH)_4(OH)_3(H_2O)_3$	(3,9)-Connected **gfy**	41
DUT-98	9-(4-Carboxyphenyl)-carbazole-3,6-dicarboxylic acid (H_3CPCDC)	$Zr_6O_4(OH)_4(H_2O)_4$	(3,12)-Connected **llj**	28
TCM-16	4,4′,4″-[1,3,5-Benzenetriyltris(ethyne-2,1-diyl)] tribenzoate (BTEB)	$Zr_6O_4(OH)_4(H_2O)_4$	(3,12)-Connected **llj**	43
MOF-1004	4,4′,4″-[1,3,5-Benzenetriyltris(ethyne-2,1-diyl)] tribenzoate (BTEB)	$Zr_6O_4(OH)_4$	(3,12)-Connected **sky**	38
UPC-158	(4,4′,4″-(1*H*-Imidazole-2,4,5-triyl) tribenzoic acid) (H_3ITTC)	$Zr_6O_4(OH)_4$	(3,12)-Connected **sky**	44
MOF-525	Tetrakis(4-carboxyphenyl) porphyrin (TCPP)	$Zr_6O_4(OH)_4$	(4,12)-Connected **ftw**	45
PCN-222	Tetrakis(4-carboxyphenyl) porphyrin (TCPP)	$Zr_6(OH)_8$	(4,8)-Connected **csq**	46
MOF-545	Tetrakis(4-carboxyphenyl) porphyrin (TCPP)	Zr_6O_8	(4,8)-Connected **csq**	45
NU-1000	1,3,6,8-Tetrakis(*p*-benzoic acid) pyrene (H_4TBAPy)	$Zr_6(OH)_8$	(4,8)-Connected **csq**	47
MMPF-6	Tetrakis(4-carboxyphenyl) porphyrin (TCPP)	Zr_6O_8	(4,8)-Connected **csq**	49
PCN-225	Tetrakis(4-carboxyphenyl) porphyrin (TCPP)	$Zr_6O_4(OH)_4$	(4,8)-Connected **sqc**	50
NU-901	1,3,6,8-Tetrakis(*p*-benzoic acid) pyrene (H_4TBAPy)	$Zr_6O_4(OH)_4(OH)_4$	(4,8)-Connected **scu**	51
NU-902	1,3,6,8-Tetrakis(*p*-benzoic acid) pyrene (H_4TBAPy)	$Zr_6O_4(OH)_4(OH)_4$	(4,8)-Connected **scu**	53
PCN-521	Tetrakis(4-carboxyphenyl) porphyrin (TCPP)	$Zr_6(OH)_8$	(4,8)-Connected **flu**	53
PCN-223	Tetrakis(4-carboxyphenyl) porphyrin (TCPP)	$Zr_6O_4(OH)_4$	(4,8)-Connected **shp**	55
PCN-224	Tetrakis(4-carboxyphenyl) porphyrin (TCPP)	$Zr_6O_4(OH)_4$	(4,6)-Connected **she**	56
PCN-625	bis[3,5-bis(4-Carboxyphenyl) phenyl] porphyrin (BBCPPP)	$Zr_6(OH)_8$	(4,8)-Connected **csq**	61
Spiro-1	(*S*)-H_4L_1	$Zr_6O_4(OH)_4$	(4,8)-Connected **sjt**	62
NU-1400	[1,1′:4′,1″]-Terphenyl-3,3″,5,5″-tetracarboxylic acid (TPTC)	$Zr_6O_4(OH)_4$	(4,4)-Connected **lvt**	64
Zr-lvt-MOF	2′,5′-Dimethyl-[1,1′:4′,1″-terphenyl]-3,3″,5,5″-tetracarboxylate (tptc-$(Me)_2$)	$Zr_6O_4(OH)_4$	(4,4)-Connected **lvt**	41
MOF-892	1′,2′,3′,4′,5′,6′-Hexakis(4-carboxyphenyl) benzene (H_6CPB)	$Zr_6O_4(OH)_4$	(4,6)-Connected **stp**	65
ACM-10	Tetrathiafulvalene tetrabenzoic acid (TTFTB)	$Zr_6O_4(OH)_4$	Two-dimensional **sql**	70
PCN-903-$(CH_3)_6$	5′,5′′′′-Methylenebis(2′,4′,6′-trimethyl-[1,1′:3′,1″-terphenyl]-4,4″-dicarboxylic acid) (L-$(CH_3)_6$)	$Zr_6O_4(OH)_4$	(4,6)-Connected **cor**	71
pbz-MOF-1	Hexakis(4′-carboxy[1,1′-biphenyl]-4-yl) benzene (HCBB)	$Zr_6O_6(OH)_2$	(6,6)-Connected **pbz**	72
PCN-136	(Hexakis(4-carboxyphenyl) hexabenzocoronene) (HCHC)	$Zr_6O_4(OH)_4$	(6,6)-Connected **pbz**	73
NU-1600	H_6PET-1	$Zr_6O_2(OH)_6$	(6,12)-Connected **alb**	74
NU-1601	H_6PET-2	$Zr_6O_2(OH)_6$	(6,12)-Connected **alb**	74
NU-1602	H_6PET-3	$Zr_6O_2(OH)_6$	(6,12)-Connected **alb**	74

topology guided by a topological design approach. The carboxylic groups in H_3CTTA and H_3TTNA are parallel to the central benzene ring because of the introduction of steric hindrance. The framework structure of BTU-12 was constructed by D_{4h} 8-connected Zr_6 clusters and D_{3h} 3-connected ligand linkers.[37–39] With the increase in connectivity of Zr_6 clusters, the symmetry of the tricarboxylate ligand decreased at the same time. To get the higher connectivity of Zr_6 clusters, Li's group revealed the first case of Zr-MOF (BUT-39) with (3,9)-connected **sep** topology *via* designing a unique low-symmetric T-shaped tricarboxylate ligand. Each H_3BTBA ligand in BUT-39 possesses both 90 and 180° bridging angles to link two kinds of crystallographically independent eight-coordinated Zr atoms and each Zr_6 cluster adopts C_3 symmetry to connect nine tricarboxylate linkers.[40] Ma and co-workers also reported another example of (3,9)-connected Zr-MOF based on C_{2v}-symmetric tridentate corrole ligand and D_{3d}-symmetric 9-connected Zr_6 clusters. The 9-connected $Zr_6(\mu_3\text{-}O)_4(\mu_3\text{-}OH)_4(OH)_3(H_2O)_3(COO)_9$ clusters in Corrole-MOF-1 are bridged by 3-connected $TCPC^{3-}$ ligands forming 3D frameworks with large hexagonal 1D open channels. Interestingly, the symmetry of the 9-c Zr_6 cluster reduced from O_h to D_{3d}, in order to compact with low symmetry tridentate corrole ligands. It should be highlighted that although BUT-39 and Corrole-MOF-1 are both (3,9)-connected Zr-MOFs, the symmetry of the ligands and connectivity of Zr_6 clusters are different from each other.[41] Apparently, it is also a great challenge to obtain (3,12)-connected Zr-MOF due to the geometry mismatch for 12-connected Zr_6 clusters and triangular ligands.[42]

Inspired by the success of reticular chemistry, when the connectivity of Zr_6 clusters and triangular ligands are fixed, one can expect to realize (3,12)-connected Zr-MOF by changing the flexibility of triangular ligands, such as the introduction of heteroatom to the rigid ligand skeleton and/or increasing the length of ligand arms. Following this criterion, Krause *et al.*

exhibited the rational synthesis of the switchable Zr-based network based on tritopic carbazole ligands. In the structure of DUT-98, two carbazole carboxylic groups in the CPCDC ligand adopt a bidentate chelation mode to the 8-connected Zr_6 nodes and the third phenylcarboxy group employed monodentate to the terminal –OH/H_2O sites of the Zr_6 nodes. DUT-98 is a flexible (3,12)-c net with llj topology. It is interesting that the structure can be switched from DUT-98*as* to DUT-98*cp* upon solvent removal and adsorption, indicating a stimuli-responsive behavior. The high structural flexibility is attributed to the conformation of the CPCDC ligand.[28] Similar 12-connected $[Zr_6(BTEB)_4(\mu_3\text{-}O)_4(\mu_3\text{-}OH)_4(H_2O)_4]$ clusters can also be found in TCM-16, where an extended tritopic carboxylate ligand ($BTEB^{3-}$) was used with benzoic acid as the modulator.[43] The $BTEB^{3-}$ ligands also exhibit a monodentate and bidentate coordination mode to link three different Zr_6 clusters. But unlike DUT-98, the structure of TCM-16 is highly augmented without solvent-dependent expand and contract behavior. Recently, using the same ligands and different reaction conditions, Yaghi reported the first (3,12)-connected sky net, named MOF-1004, which contained 12-coordinated $Zr_6(\mu_3\text{-}O)_4(\mu_3\text{-}OH)_4(\text{-}COO)_{12}$ clusters and tritopic $BTEB^{3-}$ linkers. The successful construction of MOF-1004 may contribute to the twist of longer linkers. However, because of the flexibility of $BTEB^{3-}$ linkers, they obtained the other unknown phase simultaneously accompanied by the formation of MOF-1004, which impedes further characterization and applications.[38] To further reduce the symmetry of the tricarboxylate ligand, we introduced N atoms to the ligand skeleton and an imidazole-tricarboxylate ligand (H_3ITTC) was designed and synthesized. Our group reported a new porous and stable zirconium MOF (UPC-158) with sky topology. Thus, the symmetry of the Zr_6 cluster in UPC-158 is the highest O_h symmetry and surprisingly the symmetry of the H_3ITTC ligand in UPC-158 reduced to the lowest C_s symmetry. Our research indicated that this symmetry reduction of the linker is the key factor making the triangular ligand symmetrically match the $Zr_6(\mu_3\text{-}O)_4(\mu_3\text{-}OH)_4(\text{-}COO)_{12}$ clusters.[44]

2.1.3 Zr-MOFs based on tetratopic carboxylic ligands. Aside from the above-discussed linear and tritopic ligands, the tetratopic carboxylic ligand is an integral part of constructing Zr-MOFs because of their greater number of coordination sites and abundant coordination patterns. What's more important is the rigid framework based on tetracarboxylic ligands can avoid framework interpenetration effectively to create mesoporous Zr-MOFs. As a general rule, the combination of tetratopic carboxylic ligands and Zr_6 clusters led to multiple topologies, depending on the geometry of tetratopic carboxylic ligands and Zr_6 clusters.4 For example, 4,12-c **ftw** net in MOF-525,[45] 4,8-c **csq** net in PCN-222,[46] MOF-545,[45] NU-1000,[47,48] and MMPF-6,[49] 4,8-c **sqc** net in PCN-225,[50] 4,8-c **scu** net in NU-901[51,52] and NU-902,[53] 4,8-c **flu** net in PCN-521,[54] 4,8-c **shp** net in PCN-223[55] and 4,6-c **she** net in PCN-224.[56] It has been confirmed that the linker conformation, flexibility and steric hindrance seriously influenced the final structures.[57–59] The larger hexagonal and smaller triangular channels in the **csq** topology are in favor of catalysis and related applications.[60] The porphyrin cores in PCN-222 and pyrene cores in NU-1000 are parallel to the pore surfaces of larger hexagonal channels. Very recently, our group developed another **csq** porphyrin-based Zr-MOF, PCN-625, in which the porphyrin rings are vertical to the pore walls. Compared with PCN-222, the vertical porphyrin cores, shrunken pore sizes, together with steric hindrance can impede the accessibility of substrates to active centers in the framework benefiting for size-selective catalysis.[61]

Aside from the diversities of organic linkers, the Zr clusters can also possess multiple configurations even in the same MOF. For example, Cui and coworkers reported a chiral Zr-MOF based on tetratopic chirality linkers with (4,8)-connected **sjt** topology, in which the Zr clusters adopt D_{4h} and D_{2d} symmetries in Spiro-1.[62,63] To further explore the ultimate tolerance of zirconium clusters to a defect, the coordination numbers of Zr clusters can be further reduced. With the reduction of coordination numbers, the flexibility increased. The good geometric and topological compatibility between tetracarboxylic ligands and Zr_6 clusters results in a variety of new topologies, such as (4,4)-connected **lvt** topologies in NU-140064 and Zr-**lvt**-MOF,[41] and a (4,6)-connected **stp** topology in MOF-892.[65] Thus, Zhao and co-workers reported some interesting results, including 2D nets, a two-fold interpenetrated **ftw** structure, (4,10)-connected and (4,8)-connected **sqc** nets and discrete metal–organic cage and macrocycle.[66–69] Surprisingly, Gascon synthesized two new 2D Zr-MOFs based on tetrathiafulvalene linkers with **sql** topology.[70] Thus, PCN-903-$(CH_3)_6$ was also constructed by our group with (4,6)-connected **cor** topology, in which the tetracarboxylate linkers with C_1 symmetry bridged the Zr_6 clusters with different dihedral angles.[71]

2.1.4 Zr-MOFs based on hexatopic carboxylic ligands. As far as we know, there are only two examples of Zr-MOFs constructed by hexatopic carboxylic ligands and 6-c Zr_6 clusters in pbz-MOF-172 and PCN-136. The structure of pbz-MOF-1 and PCN-136 is (6,6)-connected **hxg-a** topology. It is interesting that the structure of PCN-136 can only be obtained by aromatization-driven postsynthetic annulation because of the rigid HCHC with π-conjugation.[73] Furthermore, in order to assemble with each other, hexatopic ligands and Zr clusters have to change their connections and/or conformations. For example, when H_6CPB was used, only four carboxylates of H_6CPB coordinated with Zr_6 clusters, giving rise to (4,6)-connected **stp** and (4,8)-connected **hfp** topology. However, in Li's report, the Zr_6 clusters turn to 9-connected with a planar hexacarboxylate linker. The combination of 6-connected trigonal-prismatic linkers and 12-connected hexagonalprismatic Zr clusters yield NU-1600, NU-1601 and NU-1602 with (6,12)-connected **alb** topology. It should be highlighted that the case of Zr-MOFs based on hexatopic carboxylic ligands is still rare, due to the difficulties in synthesizing ligands and MOFs.[74]

2.2 The development of titanium MOFs

Compared with the various Zirconium-based MOFs, crystalline and porous titanium-based materials are of great interest because of their low toxicity, high natural abundance, and potential photocatalytic and redox properties.[17,75] Unfortunately, there is not yet a versatile synthetic or theoretical route for the preparation of Ti-MOFs. Table 2 lists some typical Ti-based MOFs based on carboxylate acid.

Table 2 Representative Ti-MOFs based on carboxylic ligands

Ti-MOF	Organic linker	Ti resource	Ti cluster	Ref.
MIL-125(Ti)	1,4-Benzenedicarboxylic acid (H_2BDC)	$Ti(O^iPr)_4$	$Ti_8O_8(OH)_4$	10
NH_2-MIL-125(Ti)	2-Aminoterephthalic acid ($BDC\text{-}NH_2$)	$Ti(O^iPr)_4$	$Ti_8O_8(OH)_4$	77
COK-69	1,4-Cyclohexanedicarboxylate (H_2cdc)	$Cp_2Ti^{IV}Cl_2$	Ti_3O	79
Ti-MIL-101	1,4-Benzenedicarboxylic acid (H_2BDC)	$TiCl_3$	Ti_3O	80
Ti_3-BPDC-Ir	Biphenyl-4,4′-dicarboxylic acid, H_2L_1	$Ti_6O_6(O^iPr)_6(abz)_6$	$Ti_3(OH)_2$	81
Ti_3-BPDC-Ru	Biphenyl-4,4′-dicarboxylic acid, H_2L_2	$Ti_6O_6(O^iPr)_6(abz)_6$	$Ti_3(OH)_2$	81
MOF-901	Benzene-1,4-dialdehyde (BDA) 4-aminobenzoic acid (H-AB)	$Ti(O^iPr)_4$	Ti_6O_6	83
MOF-902	4,4′-Biphenyldicarboxaldehyde (BPDA) 4-aminobenzoic acid (H-AB)	$Ti(O^iPr)_4$	Ti_6O_6	84
MIL-100(Ti)	Benzene-1,3,5-tricarboxylic acid (H_3btc)	$Ti_6O_6(4\text{-}tbbz)_6(O^iPr)_6$	Ti_3O	87
ZSTU-1	4,4′,4″-Nitrilotribenzoic acid (H_3TCA)	$Ti(O^iPr)_4$	$Ti_6O_6(OH)_6$	88
MIP-207	Benzene-1,3,5-tricarboxylic acid (H_3btc)	Ti_8AF	Ti_8O_8	89
MIP-208	Isophthalic acid (IPA)	Ti_8AF	Ti_8O_8	90
PCN-22	Tetrakis(4-carboxyphenyl) porphyrin (TCPP)	$Ti_6O_6(O^iPr)_6(abz)_6$	Ti_7O_6	91
DGIST-1	Tetrakis(4-carboxyphenyl) porphyrin (TCPP)	$Ti_6O_6(O^iPr)_6(abz)_6$	Ti-oxo chain	92
Ti-TBP	(5,10,15,20-Tetra(*p*-benzoato)-porphyrin) (TBP)	$TiCl_4{\cdot}2THF$	Ti-oxo chain	93
ACM-1	4,4′,4″,4‴-(Pyrene-1,3,6,8-tetrayl) tetrabenzoic acid (TBAPy)	$Ti(O^iPr)_4$	Ti–O–Ti chains	94
MTM-1	Isonicotinic acid (INA), cuprous iodide	$Ti(O^iPr)_4$	Ti_6O_6	95

2.2.1 Ti-MOFs based on ditopic carboxylic ligands. Serre and co-workers synthesized the first titanium carboxylate MOF using a hydrothermal method in 2009, which was constructed from a ditopic terephthalic acid linker and 12-connected $Ti_8O_8(OH)_4(COO)_{12}$ clusters.[10] Notably, the appropriate choice of DMF/MeOH solvent and titanium isopropoxide $[Ti(O^iPr)_4]$ precursor plays a major role in preparing high crystalline and porous MIL-125. Taking the high reactivity of titanium isopropoxide into account, it can be replaced by $Ti_8O_8(OOCR)_{16}$ clusters. The topology of MIL-125 can be viewed as a **fcu** net, the same as UiO-66, although the Ti_8 core is less symmetric than the Zr_6 core. Interestingly, MIL-125 shows potential photocatalysis properties *via* the transformation between Ti^{4+} and Ti^{3+}. However, different from the success of isoreticular expansion in the well-known Zr_6 cluster, the synthesis of MIL-125 isostructures using elongated ditopic carboxylic linkers and a Ti_8 cluster was unsuccessful.[76] Much attention was paid to modifying the organic ligands to tailor their photoactivities. For example, the amine functionalized BDC linker was utilized to form the NH_2-MIL-125(Ti).[77] The introduction of $-NH_2$ influences not only the charge transfer from O to Ti but also the adsorption capability toward CO_2. The optical bandgap of NH_2-MIL-125(Ti) is down to 2.6 eV, which promotes the photocatalytic reduction of CO_2 under visible light irradiation.[78] The photocatalytic activity of NH_2-MIL-125(Ti) under visible light irradiation has undergone several improvements, including post-modification using dye-like molecular fragments and encapsulating active species.[17,75]

When the connectivity of the Ti_8 cluster reduces to the Ti_3 cluster, COK-69 can be obtained based on flexible 1,4-cyclohexanedicarboxylate linkers under an inert atmosphere, in which the frequently-used $[Ti(O^iPr)_4]$ precursor was substituted by $(Cp_2Ti^{IV}Cl_2)$. COK-69 presents a flexible framework and reversible photo-activities under UV irradiation, involving simultaneous electrons and protons transfer.[79] By changing the Ti resource to $TiCl_3$, another Ti-MOF was discovered under an inert atmosphere and solvothermal conditions. The carboxylate-bridged titanium oxo clusters in Ti-MIL-101 have triangular $Ti_3O(COO)_6$ configuration with unsaturated M^{III} centers, which is similar to that in M^{III}-MIL-101. Thus, the Ti^{III} centers can further oxidize to Ti^{IV} superoxo and peroxo species.[80] Applying functionalized BPDC ligands and $Ti_3(OH)_2$ secondary building units, two new titanium MOFs, Ti_3-BPDC-Ir and Ti_3-BPDC-Ru were fabricated using a mixed ligands method. In the structure, the $Ti_3(OH)_2$ nodes come from the more stable $Ti_6O_6(O^iPr)_6(abz)_6$ precursor, affording an hourglass conformation. The incorporation of Ir and Ru endows Ti_3-BPDC-Ir and Ti_3-BPDC-Ru photocatalytic HER activities *via* excited photosensitizer quenching and electron transfer (Fig. 3a).[81] The neighbouring Ti_3 clusters can also be bridged by Co for the cascade reduction as a metal catalyst.[82] Since it still remains a challenge to find a new synthetic

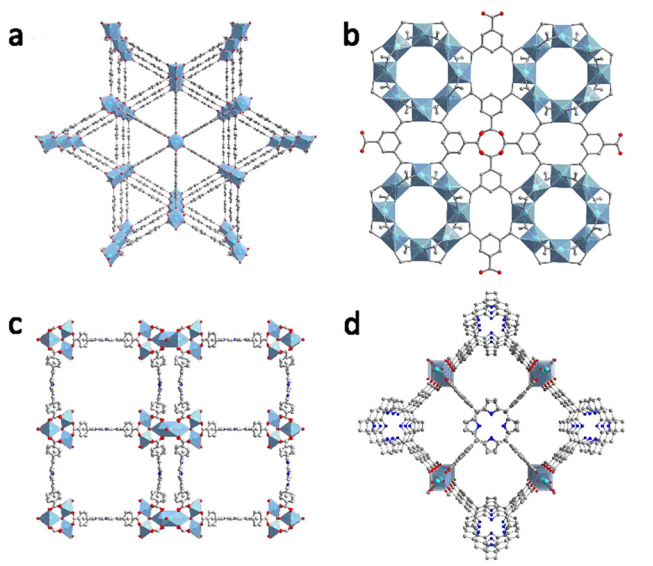

Fig. 3 (a) Ti_3-BPDC-Ir with $Ti_3(OH)_2$ SBU and ligand. Reproduced from ref. 81 with permission from the American Chemical Society, copyright 2019; (b) Ti_8O_8 core in MIP-207. Reproduced from ref. 89 with permission from the Elsevier, copyright 2019; (c) PCN-22 with a Ti_7O_6 cluster and TCPP. Reproduced from ref. 91 with permission from the Royal Society of Chemistry, copyright 2015; (d) DGIST-1 with a Ti-oxo chain. Reproduced from ref. 92 with permission from the Wiley-VCH, copyright 2018.

strategy to generate Ti-MOFs, Nguyen *et al.* developed an *in situ* cluster generation technique to synthesis MOF-90183 and MOF-902.[84] The $Ti_6O_6(O^iPr)_6(abz)_6$ cluster is generated *in situ* and reacts with carbonyl groups of linear dialdehyde linkers *via* condensation reactions. The newly synthesized covalent bonds bridge the gap between MOF and COF.[85]

2.2.2 Ti-MOFs based on tritopic carboxylic ligands. Crystalline and porous titanium-based MOFs can also be synthesized by Ti clusters and tritopic carboxylic ligands, although the quantity of Ti-MOFs is not as much as ditopic carboxylic ligands. Considering that the Ti precursors are more prone to hydrolyse into TiO_2, a postsynthetic strategy has proven to be an incredibly powerful approach for constructing and modifying Ti-MOFs. For example, Zhou's group developed a versatile synthetic route for the preparation of Ti-MOFs by metal exchange and mild oxidation. A series of Ti-MOFs based on the MIL-100(Sc) structure can be obtained, and the resulting Ti-MOFs not only maintain their crystallinity but also exhibit excellent photocatalytic properties.[86] After that, the formation of MIL-100(Ti) was systematic explored by direct synthesis. They also proved that the formation of trimeric $Ti_3(\mu_3\text{-O})$ clusters is thermodynamically favoured and revealed the importance of controlling the reactivity of Ti precursors between pre-formed clusters and organometallic complexes. The direct synthesis of Ti-MOFs avoids the incomplete metal replacement and deposition of metal oxide coatings, which are encountered in postsynthetic strategies.[87] The reaction of titanium isopropoxide with the tritopic carboxylate ligand yields three isoreticular 1D rod-based Ti-MOFs with infinite $[Ti_6(\mu_3\text{-O})_6(\mu_2\text{-OH})_6]_n$ SBUs. In ZSTU-1, the infinite Ti–O chains with hexagonal prism conformation link six tritopic carboxylate ligands.[88] Recently, in order to better control the Ti-MOF structures during direct synthesis, Serre developed a controlled synthesis strategy to build Ti-MOFs through trimesic acid linker-exchange with Ti_8AF clusters. This facile synthesis method is beneficial for scale-up preparation. Interestingly, two carboxylic groups of the BTC linker in the structure of MIP-207 participated in coordination with Ti_8O_8 clusters, leaving one free carboxylic group pointing toward the pore, which allows functional modification of the pore environment of the Ti-MOF (Fig. 3b).[89] Moreover, the same group reported another ultra-microporous Ti-based MOF (MIP-208), which was the first to be assembled from a Group 4 metal and isophthalic acid (IPA) type linker, and can be used for CO_2 photocatalytic methanation. When ruthenium oxide nanoparticles were loaded onto MOF, MIP-208@RuOx composites can effectively improve the photocatalytic performance. MIP-208 crystallized in the *I*41/*amd* space group, the Ti–O helix chain and 5-acetamidoisophthalate (5-Aa-IPA) were connected up and down to reduce steric hindrance and formed a 1D channel along the c-axis. In addition, a series of multiple MIP-208 (MTV-MIP-208) have been prepared by mixing different linkers.[90]

2.2.3 Ti-MOFs based on tetratopic carboxylic ligands. Compared with the controllable synthesis of Ti-MOFs, the development of new titanium-frameworks with a single crystal is more challenging. The multiple tetratopic carboxylic ligands may offer a chance to address these questions. For example, Zhou reported the first single crystalline titanium MOF based on tetratopic carboxylic linkers. PCN-22 was prepared by the reaction of $Ti_6O_6(O^iPr)_6(abz)_6$ and TCPP under solvothermal conditions. It is amazing that the Ti_6 clusters transformed to Ti_7 clusters. As a 6-connected node, each Ti_3O_3 connected 4-connected TCPP, forming a novel (4, 6) net. The single crystalline nature of PCN-22 promoted a better understanding of the relationship between structure and property, which will be helpful in the design and synthesis of functional titanium MOFs (Fig. 3c).[91] By optimizing the synthetic conditions, the other Ti-MOF based on TCPP was synthesized. In the structure of DGIST-1, the Ti-oxo chains are formed instead of Ti_7 clusters, which are connected by perpendicular TCPP ligands (Fig. 3d).[92] Employing $TiCl_4{\cdot}2THF$ as the Ti source, Lin prepared another Ti-MOF based on TCPP linkers. In the structure of Ti-TBP, infinite Ti-oxo chains are generated *in situ* and the coordination modes of five Ti^{4+} ions in each repeat unit of the Ti-oxo chains are different. Thus, the nano-size Ti-TBP can be applied for type I photodynamic therapy.[93] In addition, the tetratopic carboxylic ligands TCPP can be expanded to other ligands to get isoreticular Ti-MOFs, such as a TBAPY linker in ACM-1.[94] To maintain the integrity and orientation of the $Ti_6O_6(O^iPr)_6(INA)_6$ precursor, MTM-1 was solvothermally prepared by the combination of titanium(IV) isopropoxide, cuprous iodide salt and INA. The structural feature of MTM-1 is a six-connected $Ti_6O_6(O^iPr)_6(INA)_6$ cluster and 4-connected Cu_2I_2 dimer, resulting to a binodal (4,6)-connected net. For the first time, they disclosed the possibility for getting highly crystalline porous Ti-MOFs with transition metal clusters and rigid titanium-oxo clusters.[95]

2.3 The development of heterometallic Ti/Zr-oxo clusters

In 2014, Yaghi and co-workers revealed the MOF-74 with 2, 4, 6, 8, and 10 different metals, which extend the concept of MTV-MOFs from mixed-linker to mixed-metal (cluster) MOFs. Zr-MOFs are well known for their exceptional chemical and thermal stabilities arising from the strong Zr–O bonds and the high connectivity of the clusters. But, single Zr-MOFs also lack potential application, such as redox catalysis, due to the redox inert nature of Zr^{4+}. Mixing the different metal source is a kind of anticipated strategy to solve the problem and tune the desired properties. Researchers have been pursuing ways to incorporate a second metal into Zr-MOFs, especially for Ti(IV) cations.

Cohen reported the introduction of the Ti(IV) cation into the UiO-66 microcrystalline MOF using a Postsynthetic Cation Exchange method.[96] Specifically, UiO-66 microcrystalline MOF was immersed in DMF solutions with different Ti(IV) sources, such as $TiCp_2Cl_2$, $TiCl_4(THF)_2$, or $TiBr_4$. The solid-liquid PSE process was monitored by using positive-ion ATOFMS spectra and the Zr/Ti doping ratio was determined by inductively coupled plasma mass spectrometry (ICP-MS). Due to the reactivity and instability of Ti(IV) salts, the Zr/Ti doping ratio can vary from 73 to 94%. Although there is no direct single crystal evidence, all the results of PXRD, TGA, BET and color proved Zr/Ti SBU inclusion. However, their subsequent research demonstrated that the metal ion deposition on the surface of these

MOFs resulted in nanoscale metal oxides rather than swapped metal sites.[97] From the viewpoints of coordination chemistry, the Zr ions are 8-coordinated in UiO-66, which is not fit for 6-coordinated Ti. A postsynthetic cation exchange method was considered an effective route to prepare heterometallic Ti/Zr substituted MOFs.[98] Several follow-up works claimed successful Ti-exchange following Cohen's method, and Li and Cohen prepared Ti substituted NH_2-UiO-66(Zr) and mixed-ligand MOF 1(Zr/Ti) *via* a postsynthetic exchange (PSE) method and investigated their photocatalytic CO_2 reduction and hydrogen evolution activities under visible light irradiation (Fig. 4a).[99,100] The introduction of amine- and diamine-substituted ligands greatly expands the light absorption capacity, especially for visible light. Thus, embedding Ti ions into the Zr_6 SBUs of amine-substituted UiO-66 may introduce new energy levels for additional charge transfer. Both of them improve the visible light photocatalytic performance. Furthermore, Zhou developed a microwave-assisted method to introduce titanium into the UiO-66 framework, which simplifies the MOF preparation, and cation exchange for the PSM of MOFs. The as-prepared UiO-66(Zr/Ti)-M demonstrated tremendous improvement by photocatalysis reduction of Se(VI) over UiO-66.[101] This further increased the photocatalytic performance for the generation of reactive oxygen species under visible light to investigate their potential photodynamic therapy applications. Recently, Jiang and co-workers synthesized Ti and Zr mixed nanoparticles (NPs) of porphyrin MOFs (PCN-224) through a post-synthetic exchange (PSE) method. The results demonstrated that Ti incorporation into Zr SBU could significantly enhance the generation of ROS *via* increasing the electron transfer from TCPP to the Zr-Ti-oxo to eliminate MDR bacteria.[102]

Different from the post-synthetic exchange (PSE) method, Ti ions can be incorporated into Zr_6 clusters by reacting with exposed –OH/H_2O groups on the unsaturated Zr_6 clusters, instead of cation exchange and/or substitution of Zr ions.[103] Farha's group reported a (3,8)-connected Zr MOF(NU-1200) with **the** topology by introducing steric constraints to control the geometry of the organic building unit. The structure of NU-1200 consists of sodalite-like cages and inter-connected mesoporous 1D channels and all the –OH/H_2O groups on the unsaturated 8-connected Zr_6 nodes point into large channels. Based on the structure characteristics and high thermal and chemical stability, fortunately, they obtained the single crystal of NU-1200-Ti after modification by titanium isopropoxide [Ti(^{i}PrO)$_4$] in dichloromethane. SC-XRD of NU-1200-Ti definitely proved the successful incorporation of Ti into Zr_6 clusters with two Ti^{4+} atoms per Zr_6 node (Fig. 4b). So, a solvent assisted metal incorporation (SAMI) strategy demonstrated its great potential for immobilizing single site metal atoms/clusters into a rigid scaffold by using reactive metal precursors.[39] Besides embedding Ti ions into the Zr_6 SBUs, Ti ions can be decorated onto an organic linker by postsynthetic metalation with a molecular Ti(IV) precursor (Fig. 4c).[104]

As a traditional vapor-phase synthetic technique for depositing thin films, atomic layer deposition (ALD) can also be used to install metals with atomic precision into MOFs from the gas phase.[48] Different from other deposition methods, for example chemical vapor deposition/infiltration, the advantage of ALD is that precursor molecules have only self-limited deposition on the surface of the chemical reaction. Hupp and Farha developed ALD in a MOF (AIM) targeted approach to anchor bivalent, trivalent and tetravalent metal to unsaturated Zr_6 nodes without significant loss of MOF crystallinity or internal surface area.[105–108] The metal content was usually determined by inductively coupled plasma-optical emission spectroscopy (ICP-OES) and computational results. Bimetallic CoAIM-Ti(IV)SIM zirconium-containing MOF was synthesized and catalysed the oxidative dehydrogenation of propane.[109] AIM exhibits great potential applications in catalysis, sorption, and separation. However, due to the disordered distributions and low occupancy of the post-synthetically cluster metalation, it is still a great challenge to locate the structural information of the post-incorporated metal centers precisely. Zhou *et al.* investigated cooperative cluster metalation and ligand migration in a flexible Zr-MOF system, in which the cluster transformation during the metalation was monitored and tracked *via* SCXRD. They demonstrated that the success of cluster transformation and ligand migration to a great extent depends on the flexibility of PCN-700.[110] Recently, Farha reported a Zr_6Ti_4-based highly reactive biocidal photocatalyst, denoted as NU-1012, by incorporating titanium into the zirconium-pyrene-based MOF and ligand migration (Fig. 4d). Thus, it should be highlighted that the structural transformation and ligand migration pathway was different from that in a flexible PCN-700 matrix because of the rigid framework of NU-1012. Moreover, this kind of straightforward Ti post-synthetic metalation strategy can be extended to any Zr-MOFs with a specific structure.[111]

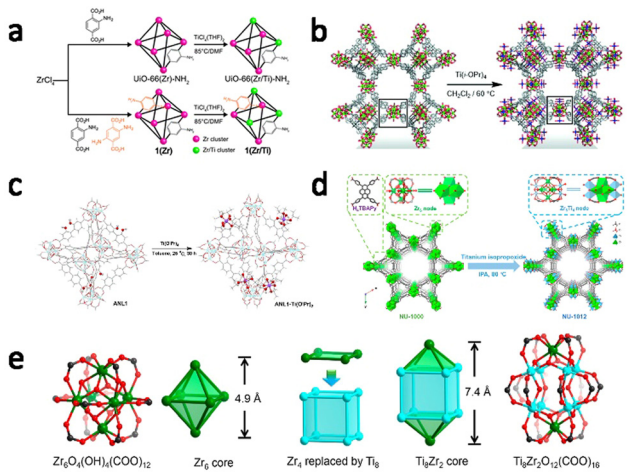

Fig. 4 Illustration of heterometallic Ti/Zr-MOFs (a) postsynthetic cation exchange. Reproduced from ref. 100 with permission from the Royal Society of Chemistry, copyright 2015; (b) incorporated into Zr_6 clusters. Reproduced from ref. 39 with permission from the Wiley-VCH, copyright 2016; (c) organic linker by postsynthetic metalation. Reproduced from ref. 104 with permission from the American Chemical Society, copyright 2017; (d) ligand migration. Reproduced from ref. 111 with permission from the American Chemical Society, copyright 2022; (e) bimetallic [$Ti_8Zr_2O_{12}$-$(COO)_{16}$] cluster. Reproduced from ref. 112 with permission from the American Chemical Society, copyright 2018.

The appearance of a bimetallic $[Ti_8Zr_2O_{12}\text{-}(COO)_{16}]$ cluster addressed the synthetic difficulties of Ti-MOFs to some extent, which are derived from the incompatibility between the synthesis of the Ti cluster and MOF.[76,112] Compared to well-known $[Zr_6O_4(OH)_4(COO)_{12}]$ clusters, the robust $[Ti_8Zr_2O_{12}\text{-}(COO)_{16}]$ clusters can be viewed as replacing four equatorial Zr^{4+} by a Ti_8-cube (Fig. 4e). PCN-415 and PCN-416 were obtained by using $[Ti_8Zr_2O_{12}\text{-}(COO)_{16}]$ clusters as a precursor and the structure of them was solved by continuous rotation electron diffraction (cRED) and Rietveld refinement against synchrotron PXRD data. Through Ti/Zr doping at the atomic level, both of them exhibited excellent chemical stability and good photocatalytic activity. The use of $[Ti_8Zr_2O_{12}\text{-}(COO)_{16}]$ clusters will open up a new avenue to construct various robust and photoactive MOFs.

3 MTV-MOFs, MOF composites and derivatives

MTV-MOFs with synergistic functionalities in a designed cavity are particularly interesting because of their potential applications in gas adsorption, separation, cooperative catalysis, and biomimetics.[113] In this section, we will describe the development of MTV-MOFs. Pioneering work has been demonstrated by Yaghi and co-workers by incorporating up to eight functional groups into MTV-MOFs, which showed emergent properties distinct from their parent frameworks.[114] Thus, Tefel *et al.* demonstrated a strategy to incorporate different functional groups on linkers of various connectivity and symmetry in pre-determined positions of a mixed-linker MOF.[115–117] Zhou's group developed a sequential linker installation strategy and succeeded in the construction of MTV-MOFs by inserting one to three different linkers.[26,27] Thus, N. Stock *et al.* developed the syntheses of bimetallic Ce/Zr-UiO-66 and Ce/Zr-MOF-808 to combine the stability of Zr-MOFs and the redox activity of Ce^{4+}.[118] MTV-MOFs in this part will be described as either mixed-linker and mixed-cluster MOFs. In addition to pristine MOFs, Zr- and Ti-based MOF composites and derivatives are also involved.

3.1 Mixed-linker Zr-MOFs

At the early stage, MOFs were built by only a single metal and organic linker, which makes predicting and understanding the structure easy, but impedes the application scope of MOFs, especially for synergetic catalysis.[119] Yaghi and Kitagawa also predicted that future MOF materials will have multiple components for various functionalities.[1,120] An effective strategy for constructing multifunctional MOFs is to form MTV-MOFs, applying organic linkers with a similar length, geometry, and connectivity but different functional groups.[114] Following this, few kinds of mixed-linkers with different sizes and functional groups can also be incorporated into a MOFs skeleton. For example, TCPP ligands can be integrated into UiO-66 successfully without changing their crystal structure, morphology and stability.[121] However, the random distributions of mixed-linkers make the structural characterization difficult. In order to overcome the limitation of placing different functionalized linkers (or metals) in exact positions throughout the MTV-MOF crystal, Tefel *et al.* demonstrated a strategy to incorporate different functional groups on linkers of various connectivity and symmetry in pre-determined positions of a mixed-linker MOF. Recently, they established multicomponent MUF-77 with white-light emission by linker modification, inter ligand energy transfer, and guest binding.[117] This strategy calls for judicious choices of linkers and nodes of varying symmetry and connectivity. Recently, Qin and Lan reported PCN-138 through geometric accumulation based on triangular TBTB and square TCPP ligands. The framework of PCN-138 was a (3,4,12)-connected **urr** net.[122] In order to locate the position of functional groups, Zhou's group developed a sequential linker installation strategy and succeeded in constructing various tertiary and quaternary MOFs by inserting one to three different linkers.[123] After that, the other example of a quinary MOF with an ordered arrangement of framework fragments was revealed by Zhang's group.[124]

3.2 Mixed-cluster Zr-MOFs

In 2014, Yaghi and co-workers reported that the MOF-74 contained 2, 4, 6, 8, and 10 different metals, which pushed the concept of MTV-MOFs from mixed-linkers to mixed-metal (clusters) MOFs.[125,126] Zr-MOFs are well known for their exceptional chemical and thermal stabilities because of the strong Zr–O bonds and the high connectivity of the clusters. However, single Zr-MOFs always lack potential application. Mixing the different metal source is a kind of anticipated strategy to solve the problem and tune the desired properties. Many efforts have been devoted to incorporating a second metal in Zr-MOFs with different valence state, using a post-synthetic metal substitution approach, such as Hf^{4+} and V^{5+} ions and Zn^{2+} and Al^{3+} ions in NU-1000.[127] Besides Ti^{4+} ions, the construction of rare-earth metal–organic frameworks (RE-MOFs) is of great interest for their luminescent applications. The high connectivity of RE clusters provides a highly tunable platform to design intriguing structures through thermodynamics analysis.[128] For example, 12-connected hexanuclear RE cluster $RE_6(OH)_8(COO)_{12}$, formed in the presence of 2-fluorobenzoic acid (2-FBA) as the modulator, is quite similar to the 12-connected hexanuclear Zr cluster $Zr_6(OH)_8(COO)_{12}$. Eddaoudi *et al.* reported many Rare-Earth polynuclear MOFs with abundant topologies employing 2-fluorobenzoic acid (2-FBA) as the modulating reagent, including **fcu**-MOFs based on linear ligands, **pek**, **aea** and **gea** net with 3-connected organic ligands, **ftw** and **shp**-MOFs with quadrangular tetracarboxylate ligands and **alb**-MOF with hexacarboxylate organic ligands.[129] Because of the similarity between Zr and RE ions, it is possible to have mixed-cluster MOFs, especially for Ce ions.[130]

Using a Ce^{3+} salt, Serre *et al.* demonstrated 5% Ce^{3+} can be doped into Zr-UiO-66.[131] Bandosz and co-workers incorporated 13.3% and 7.09% of Ce^{3+} into Zr-UiO-66 and Zr-UiO-67 using $CeCl_3$, respectively, which increased the adsorption of NO_2.[132] It gains a promising expectation to mix Zr^{4+} with Ce^{4+} due to the similar ionic radius and topology. N. Stock *et al.* synthesized

Ce-MOFs with hexanuclear clusters and the presence of Ce^{4+} ions was proved by XANES experiments.[133] Moreover, they developed the syntheses of bimetallic Ce/Zr-UiO-66 and Ce/Zr-MOF-808 to combine the stability of Zr-MOFs and the redox activity of Ce^{4+}. This promising approach guarantees getting various molar ratios of Ce^{4+} to Zr^{4+} in 15–20 minutes.[118] The same group used extended X-ray absorption fine structure spectroscopy to reveal the exact stoichiometry of Ce_xZr_{6-x} cornerstones in mixed-metal UiO-66. On the one hand, they offered direct proof for the presence of both metals in a single cornerstone, on the other hand, it provided an opportunity in the construction of hierarchically porous MOFs through cluster labilization.[134] Recently, Zhou's group developed a kinetic analysis method to guide the retrosynthesis of MTV-MOFs, in which up to three different metals and two different linkers can be subsequently incorporated.[135]

3.3 Zr- and Ti-based MOF composites and derivatives

Accordingly, the catalytic active sites of Zr- and Ti-based MOFs mainly originate from unsaturated metal clusters and functional organic ligands. For example, Zr(IV) ions in NU-1000 can serve as a Lewis-acidic to canalize hydrolysis of phosphate ester.[136] A single-atom Cu(I) catalyst can be covalently attached to the defect sites of UiO-66 for the oxidation of CO with excellent selectivity.[137] Thus, a variety of functional groups and molecular catalyst ligands can also be designed and synthesized to build multi-functional MOFs, such as porphyrin, pyrene, salen and so on.

To overcome the disadvantage of pristine MOFs, because of the tunability of pore features, Zr- and Ti-based MOFs are the appropriate host materials for incorporation of guest molecular species, including metal complexes, enzymes, polyoxometalates and metal NPs (MNPs). A synergistic catalytic system can be established based on the resulting guest@MOFs and/or guest/MOFs composite material. For example, Pt@UiO-66-NH_2 and Pt/UiO-66-NH_2, Pt@MIL-125/Au and Pt/MIL-125/Au composites were employed as photocatalysts for H_2 production by microenvironment modulation. The difference of catalytic activities indicates that the location of the catalyst relative to MOFs exhibits a significant role. Furthermore, the construction of MOF-based hierarchically porous materials boosts the further applications of Zr- and Ti-based MOF composites.

As a kind of crystalline porous material with various and customizable structures, Zr- and Ti-based MOFs provide an inherent condition as precursors for preparing porous carbon-based materials or metal (oxide)/carbon nanocomposites through pyrolysis, and their porosity and long-range structural order can be partially retained.[138] Therefore, the destruction of coordination bonds reinforces the stability of MOF derivatives, which are suitable for catalytic reactions under harsh conditions. For example, the PCN-224-templated porous carbon material exhibits superior activity in the catalytic reduction of 4-nitrophenol to 4-aminophenol.[139] Four single-atom electrocatalysts derived from multivariate Zr-MOFs were employed in electrocatalytic CO_2 reduction, in which Ni_1–N–C demonstrated excellent CO FE at low CO_2 pressures.[140]

4 Catalysis

Actually, the structures of MOFs can be regarded as infinite frameworks of homogeneous catalysts, which are similar to transition metal complexes. In addition, the periodic structure of MOFs facilitates dispersing active sites uniformly throughout the framework and the porosity can profit from the accessibility of active sites and the transport of catalytic substrates/products in MOFs. At the same time, MOFs can be recycled after catalytic runs, which enables MOFs as heterogeneous catalysts. Therefore, MOFs integrate all the advantages of a homogeneous catalyst and heterogeneous catalyst.

4.1 Thermal catalysis

Compared with traditional porous materials (activated carbon, zeolite, *etc.*), the periodic framework structure and definite pore environment of MOFs can not only make the reactant have contact with the active substance quickly, but also accelerate the diffusion of the substrates and products. Therefore, MOFs as heterogeneous catalysts have been extensively explored in various chemical reactions. For example, Cao *et al.* introduced a porphyrin ligand (TCPP) into UiO-66 (Im-UiO-66) containing an imidazole functional group through a continuous post synthesis ionization and metallization method to obtain a series of multi-component MOFs, which can be used to catalyze the CO_2 cycloaddition reaction (Fig. 5). In their work, ZnTCPP⊂(Br^-)Etim-UiO-66 showed excellent catalytic performance due to the synergistic effect of Br^- and Lewis acidic Zn^{2+}.[141] Indeed, heterogeneous catalysis can be customized by combining different functional groups in organic linkers. For example, Farha's group introduced additional functional groups into the ligands to regulate their steric hindrance, resulting in Zr-MOFs with multiple topologies for catalytic CO_2 cycloaddition to styrene oxide.[142]

Our group built a cooperative catalytic system based on a Lewis acidic catalyst and nucleophilic cocatalyst by insertion and post-modification of an auxiliary (Fig. 6). In PCN-222, 8-c Zr

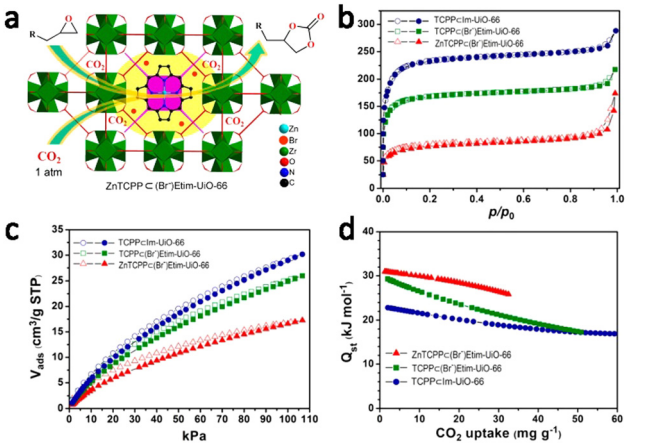

Fig. 5 (a) Schematic diagram of epoxide and CO_2 reaction with ZnTCPP⊂(Br^-)Etim-UiO-66; (b) N_2 adsorption isotherms at 77 K; (c) CO_2 adsorption isotherm at 298 K; (d) the Q_{st} for CO_2 sorption under low coverage of samples. Reproduced from ref. 141 with permission from the American Chemical Society, copyright 2018.

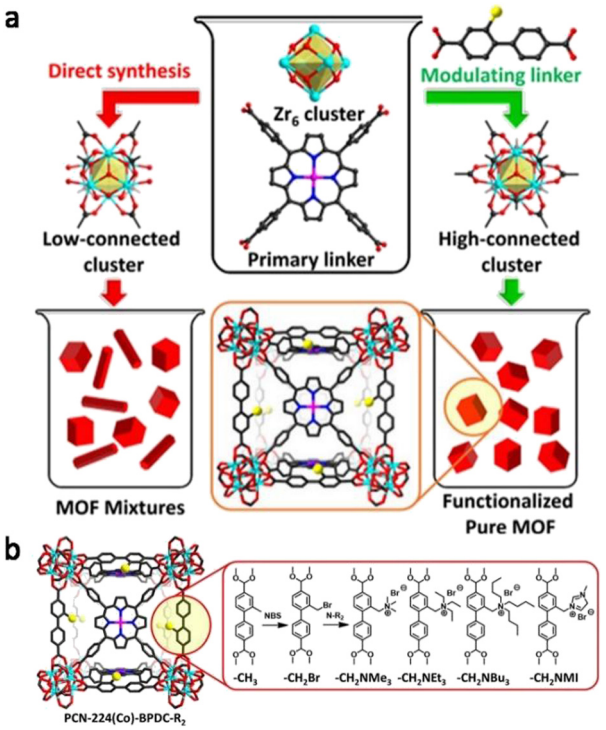

Fig. 6 (a) Synthesis diagram of an auxiliary ligand modified MOF. (b) The co-catalytic system of CO_2 epoxide cycloaddition reaction was constructed by adding different ammonium bromide to the auxiliary ligands. Reproduced from ref. 143 with permission from the American Chemical Society, copyright 2019.

clusters along the *c*-axis can accept a linear ligand NDC of similar size, forming 10-c PCN-222-NDC (NDC = 2,6-naphthalenedicarboxylate). Similarly, 6-c clusters in PCN-224 can include ligand BPDC to gain PCN-224-BPDC (BPDC = 4,4′-biphenyldicarboxylate). The addition of auxiliary ligands can not only control the formation of MOFs, but also advance the functionalization of MOFs. In PCN-224-BPDC, bromide could be attached to the BPDC to boost the cyclic addition reaction of CO_2 with epoxides. Among the different substituents shown in Fig. 6b, the maximum conversion rate (99%) was obtained for $-CH_2NBu_3$, which was due to the fact that the large substituents can cause the bromide to be far away from quaternary ammonium cations, thus enhancing their reactivity.[143] Afterwards, they also designed and synthesized a new porphyrin Zr-MOF for heterogeneous catalysis of size selective [4+2] hetero-Diels–Alder cycloaddition reaction.[61] Considering the importance of metal nanoparticles in the heterogeneous catalysis of MOFs, our team constructed Pd@UiO-66-X composites by encapsulating Pd nanoparticles in UiO-66-X (X = H, NH_2, 2OH, 2OH(Hf), OMe), which can effectively catalyse the hydrogenation of benzoic acid. Pd@UiO-66-OH showed the best catalytic activity due to the different charge transfer between MOFs and Pd and the substrate adsorption energy ($-H > -OMe > -NH_2 > -2OH(Hf) > -OH$).[144]

According to the ligand design strategy, Liu *et al.* directly combined the chiral phosphoric acid catalyst with MOF to effectively prevent its coordination with metal ions, and thus obtained a pair of chiral Zr-MOFs that were beneficial to catalyse asymmetric tandem reactions. Based on the potentially active Lewis-acid sites of Zr-oxo clusters, these two chiral MOFs exhibited high activity and enantioselectivity in organic catalytic reactions. In the enantioselective tandem two-component condensation and cyclization of 2-aminobenzamide and aldehyde, when 1.4 mol% Spiro-1 was loaded, the condensation/amine addition reaction of 2-aminobenzamide and 4-bromobenzaldehyde produced 2,3-dihydroquinazolinone with the yield and ee up to 99% and 96%, respectively. In the catalytic condensation/amine addition reaction of 2-aminobenzylamide and aromatic aldehydes, the yield of spiro-2 remained at almost 99% and reached 80–90% ee within 10 h. Besides, in enantioselective tandem three-component Friedel-Crafts reactions of indole, aldehydes and *p*-toluenesulfonamides, these two chiral MOFs can catalysis the condensation of aromatic aldehydes with *p*-toluenesulfonamides to produce 3-indolemethanamine derivatives.[62] The catalytic transfer hydrogenation has the potential to convert biological carbonyl into the corresponding alcohols. For example, Hwang and co-workers determined that Zr-MOFs can be used for catalytic furfural to furfuryl alcohol. In their study, MOF-808 was synthesized using a solvothermal method, and after activation with methanol, the structure around MOF changed, and M-MOF-808 was generated. The furfuryl alcohol yield of M-MOF-808 was up to 85.5% compared with that of MOF-808(25.4%) at 40 °C.[145]

Nerve agents such as Sarin (GB), VX, and Soman (GD) are highly toxic chemicals that can cause fatal injuries to humans. MOFs are used as heterogeneous catalysts to effectively convert toxic substances into non-toxic products due to their adjustable structure. Previously, Farha's group investigated a series of Zr-MOFs for the hydrolysis of DMNP.[64,146,147] Then they discovered that altering the regulator would change the MOFs' surface hydrophobicity, for example, the hydrophobicity of MOF-808-X (X = OH, FA, AA and TFA) would increase with the change of the regulator FA (formic acid), AA (acetic acid) and TFA (trifluoroacetic acid), while MOF-808-OH without the regulator was the most hydrophilic. The DMNP products catalyzed by MOF-808-X in the liquid were dimethyl phosphate (DMP) and 4-NP, while in the solid state, additional by-products would be obtained, and the different regulators gave the products different selectivity. They observed that in alkaline aqueous solution, excessive OH^- would instantly replace the regulator connected with Zr_6 nodes, and eventually form MOF-808-OH, which would result in almost instantaneous hydrolysis of DMNP and complete conversion within a few minutes. In the solid state, the regulator connected by MOF-808-X and Zr_6 nodes was not easily replaced, resulting in a slow reaction speed, because MOF-808-X needs to be replaced by MOF-808-OH to promote the binding of Zr_6 nodes with organophosphorus substrates.[148] Recently, Stylianou *et al.* synthesized a series of MOF@polymer beads using a reverse rotation technique. These compounds also effectively facilitate the hydrolysis of DMNP.[149] Additionally, the surface of UiO-66_NH_2 was modified with oleic acid (OA) to increase its dispersibility in solution and then integrated into polyacrylonitrile (PAN) polymer by electrospinning to form the OA-UiO-66_NH_2/PAN that can be used for

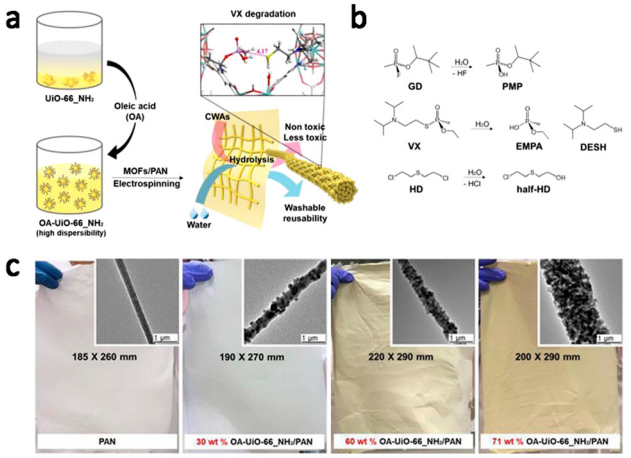

Fig. 7 (a) Illustration of hydrolytic nerve agents with an OA-UiO-66_NH_2/PAN fibrous mat. (b) Examples of degradation of CWAs. (c) Photos of fibrous mats with different contents of OA-UiO-66_NH_2 NPs (0, 30, 60 and 71 wt%). Reproduced from ref. 150 with permission from the American Chemical Society, copyright 2022.

catalytic hydrolysis of VX (Fig. 7). As shown in Fig. 7c, MOF NPs could be uniformly dispersed in PAN. With the increase of MOF NP load, the color of fiber mats gradually turned yellow, and the surface of the PAN polymer fiber changed from smooth to continuous dense morphology. With this method, large scale MOFs/polymer fibrous mats can be prepared, which is of great significance for the preparation of military/civil protective articles.[150]

4.2 Photocatalysis

In view of the dire global resource and environmental issues, how to efficiently convert solar energy into usable chemical energy has been pursued by researchers. In recent years, MOFs have been widely investigated in hydrogen production, CO_2 reduction, hydrolysis, degradation of organic pollutants and diverse organic reactions due to their controllable structure and fascinating properties. In this section, we will put our eyes on the recent development of MOFs in these fields.

The hydrogen production with MOF catalysts has attracted more and more scientists due to the practical application potential of H_2. In this respect, Ti-based MOF is reputed to be a powerful candidate material according to its excellent photochemical property and oxidation reducibility. Based on the development of discrete Ti–O clusters, Chen *et al.* predicted that the electron mobility of Ti–O rods might be higher than that of discrete Ti–O clusters. Therefore, Ti-MOF synthesized from infinite 1D rods was used for photocatalytic hydrogen release. Under the irradiation of visible light, the photocatalytic H_2 evolution rate was ZSTU-3 > ZSTU-1 > ZSTU-2. ZSTU-2 displayed the lowest photoactivity because of its poorer absorption of visible light than ZSTU-3 and ZSTU-1, while the highest activity of ZSTU-3 was due to the enhancement of light absorption and charge separation caused by the expansion of H_3BTCA ligand.[88] Considering the condition sensitivity of Ti-MOF and the catalytic performance of Zr-MOF, a bimetallic [$Ti_8Zr_2O_{12}(COO)_{16}$] cluster consisting of Zr and Ti was introduced. The resulting MOF can effectively promote the H_2 generation rate after modification with –NH_2.[112] In addition to the use of amino groups to promote photoactivity, our group reported the first broadband spectrum responsive MOF composites, UCNPs-Pt@MOF/Au (UCNPs represent upconversion nanoparticles), which revealed outstanding hydrogen production activity from the ultraviolet to the near-infrared (NIR) region. Among them, plasma Au responded to visible light, MOF mainly absorbed UV, while UCNPs could capture NIR light and convert it into visible and UV light. In addition, the core–shell structure of the hybrid could accelerate the binding of the substrate/product to the active site of Pt, increasing the catalytic activity (Fig. 8).[151]

Most water splitting involves different sacrificial agents that consume the hole to improve photocatalytic performance, and we have for the first time realized the combination of hydrogen evolution and organic conversion into the reoxidation cycle. When MOF was stimulated by light, the holes would facilitate the oxidation of benzylamine into *N*-benzylbenzaldimine, and the electrons could accelerate the reduction of protons to produce H_2.[152]

Another significant strategy for achieving efficient photocatalysis is the construction of a heterojunction. A series of Na_x-C_3N_4/Pt@UiO-66 heterojunction composites based on the advantages of Na_x-C_3N_4 and MOF were constructed, which can effectively photocatalyze H_2 production. It is noteworthy that energy level matching and visible light collection between heterojunction components can be flexibly adjusted with the change of Na concentration. $Na_{0.02}$-C_3N_4/Pt@UiO-66 had the best photocatalytic performance and the H_2 production rate reached 471.4 μmol h^{-1} g^{-1}.[153] The multiple interfaces in the Ti_3C_2/TiO_2/UiO-66-NH_2 hybrid also enhanced the separation between the charge and hole, and allowed the photogenerated electron storage of Ti_3C_2. Therefore, the synergistic effect among the three components is conducive to efficient photocatalysis,

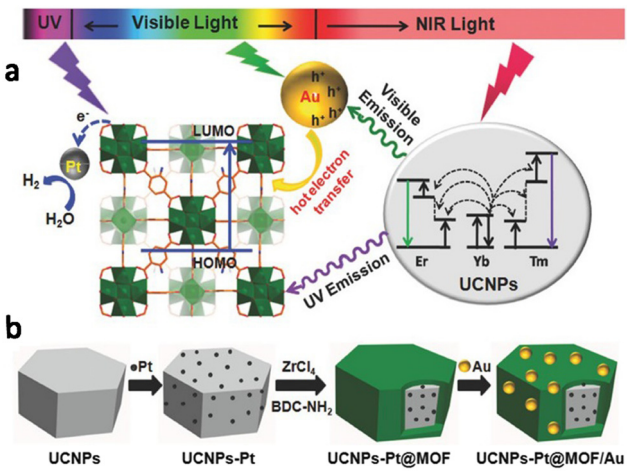

Fig. 8 (a) Illustration of the process for photocatalytic H_2 production. (b) Schematic diagram of the formation for UCNPs-Pt@MOF/Au. Reproduced from ref. 151 with permission from the WILEY-VCH, copyright 2018.

and the H_2 evolution rate of Ti_3C_2/TiO_2/UiO-66-NH_2 up to 1980 μmol h^{-1} g^{-1}.[154]

Different surface structures always show distinct catalytic activity. For example, Sun and colleagues have theoretically calculated the surface structure of NH_2-MIL-125, and found that compared with {001}, {100} and {111}, the sample with the {110} facet showed the best H_2 evolution activity and apparent quantum yield, which can be attributed to more active sites being exposed to the {110} facet.[155] Moreover, undesirable structural defects can not only regulate the band structure and conductivity of semiconductors but also provide active sites, which is undoubtedly another way to promote photocatalysis. For instance, our research group studied the influence of photoactivity caused by structural defects *via* adjusting the content of the regulator. Appropriate structural defects can facilitate the charge–hole separation and promote photocatalytic activity, among which Pt@UiO-66-NH_2-100 represented the best photocatalytic activity. The importance of structural defects on photocatalytic behaviour was systematically analysed, which laid a solid foundation for the development of semiconductor photocatalyst materials.[156]

To overcome the recombination of photogenerated electrons at single metal sites in MOFs, another effective approach is to combine metal complexes as promoters with MOFs to provide polymetallic sites to boost charge separation. By incorporating Co^{2+}, Cu^{2+} and Ni^{2+} into the Ti-MOFs, Neppolian *et al.* exhibited that the solar to hydrogen evolution (STH) efficiency of Cu-MOF was approximately 11.5 times higher than that of pure Ti-MOF.[157] We put transition metal phosphates (TMPs) in UiO-66-NH_2 to achieve high H_2 evolution activity. It was found that TMPs exhibited similar behaviour to Pt both kinetically and thermodynamically, greatly promoting charge separation and reducing the formation energy of H_2. Interestingly, Ni_2P was more prone to produce H_2 than Pt kinetically, resulting in the photoactivity of Ni_2P@UiO-66-NH_2 exceeding that of Pt@UiO-66-NH_2.[158] In addition, we assembled a series of M_1/SnO_2/MOF heterojunctions (M = Pt, Cu, and Ni), which showed superior activity over the relevant metal NPs and other complexes due to the full utilization of metal monatomic catalysts. What's more, the binding energy between different types of single atoms and hydrogen was not consistent, so the order of H_2 production rate was: Pt_1/SnO_2/UiO-66-NH_2 (2167 μmol g^{-1} h^{-1}) > Cu_1/SnO_2/UiO-66-NH_2 (1265 μmol g^{-1} h^{-1}) > Ni_1/SnO_2/UiO-66-NH_2 (654 μmol g^{-1} h^{-1}).[159] Lastly, the PdTCPP⊂PCN-415(NH_2)/TpPa complexes with excellent photocatalytic H_2 production behavior provided a path for other MOFs/COFs hybrids in this field(Fig. 9).[160] Based on the fact that the surfactant on the co-catalyst can change the chemical environment around the active site, our group investigated the interface effect of the co-catalyst (Pt) and surfactant (polyvinylpyrrolidone) on the photocatalysis by changing the amount of PVP in the complex. Surprisingly, PVP would hinder the electron transfer between Pt and MOF, and the H_2 production rate was as follows: Pt@UiO-66-NH_2 > Pt_{rPVP}@UiO-66-NH_2 > Pt_{PVP}@UiO-66-NH_2 > UiO-66-NH_2.[161]

Apart from the above strategies of crystal facet engineering, defects, cocatalyst and heterojunction construction, some metal

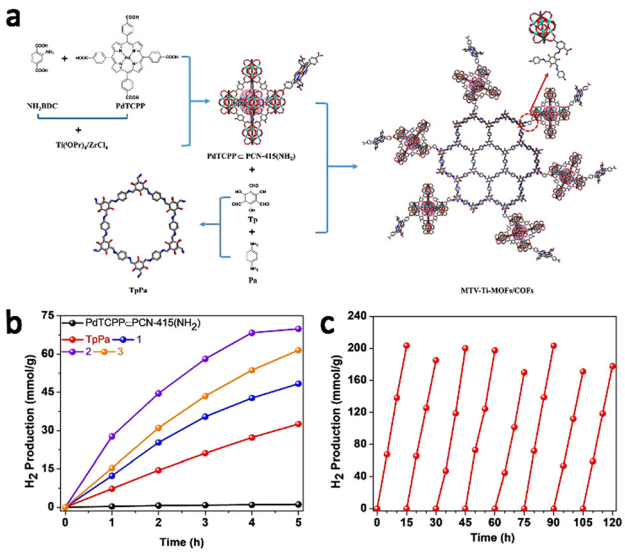

Fig. 9 (a) The schematic composition of MTV-Ti-MOFs/COFs. (b) The photocatalytic H_2 production of different catalysts. (c) Cycle test for H_2 production of composite 2. Reproduced from ref. 160 with permission from the WILEY-VCH, copyright 2021.

oxides can be used to regulate the energy band structure of photocatalysts, thereby inhibiting the recombination of electrons and holes. Our research group integrated MoO_3 and V_2O_5 onto MIL-125-NH_2 respectively, which caused the band bending of MOF hybrids, so that an internal electric field was formed near MOF to promote charge separation. Therefore, the composites represented more than 40 times higher photocatalytic activity than the original MOF.[162]

MOFs catalytic decomposition of organic pollutants under UV/vis irradiation is a green route of wastewater treatment.[163] For example, the TiO_2/MOF heterojunction can reduce the recombination of holes and photogenerated electrons, so TiO_2/ZrO_2 can achieve highly efficient photocatalytic degradation of Rhodamine B, and maintain the 90% degradation rate after four cycles.[164] Recently, Lu *et al.* proposed that the MOFs@COFs Z-heterojunction hybrid can efficiently degrade bisphenol A (BPA) due to its appropriate band gap and abundant active sites. In all samples tested, NM-125(Ti)$_{0.4}$@TpTta-COF was able to adsorb and degrade 100 ppm BPA in ten minutes.[165] MOF catalysts can not only destroy organic pollutants, but also be widely used in several organic reactions. The single crystal Ti-MOF (DGIST-1) with an infinite Ti-oxo chain could oxidize benzyl alcohol to produce benzaldehyde under visible light irradiation, and the conversion rate of benzyl alcohol catalysed by DGIST-1 reached 93% without the assistance of a cocatalyst.[92] Ye *et al.* prepared three different structures of Ir(III)–Zr(IV) MOFs by changing the organic ligands, which can be used as catalysts to effectively oxidize sulfide to sulfoxide in water upon visible light irradiation. The results showed that the catalytic efficiency of Zr_6-Irphen was up to 100% without any structure change after 10 cycles (Fig. 10).[166] By constructing a MOFs/nanoparticles (NPs)/COFs sandwich structure, Ti-MOF@Pt@DM-LZU1 catalysed more than 99% styrene to generate ethylbenzene and the turnover frequency (TOF)

was up to 577 h^{-1} under light conditions.[167] Based on the promising photocatalytic behavior of Zr-MOFs and CdS, a CdS@Zr-MOF composite was synthesized by Hou *et al.* for photocatalytic preparation of imines.[168]

The discussion of MOF catalysts provides a tempting strategy for efficiently capturing CO_2 and converting it into valuable products. By incorporating BDC-NH_2 into Ti-MOF, Fu *et al.* realized the first reduction of CO_2 by MOFs under visible light irradiation.[78] Since then, MOF catalysts have jostled for a place in this sky. For instance, we trapped Pd_3Cu in UiO-66 to synthesize Pd_3Cu@UiO-66 for carbon dioxide hydrogenation to methanol. Under the photo-assisted condition, the CH_3OH generation rate of Pd_3Cu@UiO-66 reached up to 340 μmol g^{-1} h^{-1}. Compared with Pd_3Cu/UiO-66, Pd_3Cu@UiO-66 boosted the contact between Zr-O clusters and Pd_3Cu active sites and greatly enhanced the interaction between H_2 and CO_2.[169] In addition, the spaces between porphyrin rings in Zr–polyphenolate–porphyrin MOFs with high chemical stability were divided into many pitfalls for anchoring carbon dioxide, resulting in enhanced CO_2 adsorption quantity. Meanwhile, introducing metal into porphyrin nuclei could significantly promote the photocatalytic effect. Among them, ZrPP-1-Co catalysed CO_2 reduction to produce CO at a rate of 14 μmol g^{-1} h^{-1}.[170] In view of the uncontrollability of low core Ti-MOF, only a few single crystals of Ti-MOF refer to single crystal XRD analysis, Zhang and co-workers assembled a series of large Ti-MOFs (the maximum about 100 μm) by connecting large-scale Ti_{44}-oxo clusters and organic ligands, and verified the photocatalytic performance of FIR-125 in the CH_3CN/H_2O/TEOA system. After 5 hours of visible light irradiation, the CO output could reach up to 2213.8 μmol g^{-1}.[171] Recently, Cu nanoclusters (NCs) have been encapsulated in Zr-MOFs to gain a core–shell structure, which would effectively solve the problems of NPs leaching and substrate diffusion blocking, and promote the CO_2 photoreduction performance. As shown in Fig. 11, the photocatalytic reduction of CO_2 by Cu NCs@MOF-808 mainly consisted of 64.9% HCOOH (94 μmol h^{-1} g^{-1}) and 22.5% CO (32 μmol h^{-1} g^{-1}), and while using Cu NCs@UiO-66-NH_2 as the catalyst, the HCOOH production rate increased to 128 μmol h^{-1} g^{-1} due to CO_2-NH_2 interaction. Furthermore, the core–shell construction was indeed conducive to achieving a significant catalytic performance compared to Cu/MOF.[172]

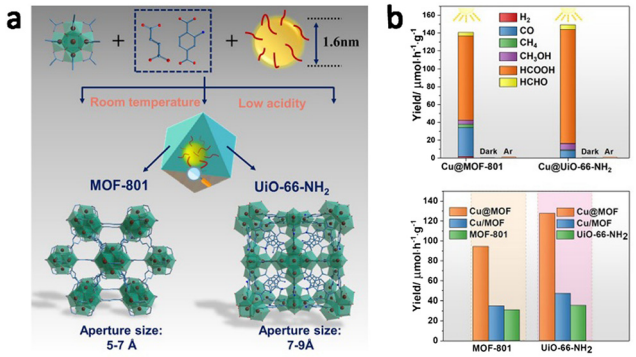

Fig. 11 (a) Illustration of Cu NCs encapsulated in Zr-MOFs. (b) Photocatalytic reduction of CO_2 by Cu NCs@Zr-MOFs and the corresponding HCOOH production rates with Cu NCs@Zr-MOFs and Cu/MOFs, respectively. Reproduced from ref. 172 with permission from the Wiley-VCH, copyright 2022.

4.3 Electrocatalysis

In recent years, MOF materials have been applied in electrocatalysis due to the favorable proton transport brought by the large specific surface area and abundant pore environment. In order to deal with the increasingly severe energy issues, electrocatalytic hydrogen evolution is undoubtedly a simple and effective way. For example, MoS_x-Fe@UiO-66-$(OH)_2$ was formed by anchoring amorphous molybdenum sulfides (a-MoS_x) on a Zr-MOF surface with a wet chemical method. Thanks to the synergistic effect between Zr-MOF and a-MoS_x, the hybrid displayed excellent HER activity under acidic conditions. Compared to MoS_x-Fe and UiO-66-$(OH)_2$, the overpotential of MoS_x-Fe@UiO-66-$(OH)_2$ was only 118 mV at 10 mA cm^{-2}. Its catalytic effect was better than Pt/C even when the current density surpassed *ca.* 225 mA cm^{-2}. Moreover, the electrochemical impedance spectroscopy (EIS) and other electrochemical data demonstrated the surprising electrocatalytic behavior of MoS_x-Fe@UiO-66-$(OH)_2$ (Fig. 12).[173]

Considering that the periodic frameworks restrain the aggregation of metal sites during MOF pyrolysis, MOFs can be used as a precursor to prepare highly conductive MOF derivatives. Our group used PCN-222 as a precursor (1D mesoporous channel), and obtained a series of Fe_x-PCN-222 (x%: the mole percentage of Fe-TCPP) by regulating the proportion of mixed ligand of Fe-TCPP and H_2TCPP. After pyrolysis, Fe_{SA}–N–C (SA represented the single atom) was formed, which displayed magnificent oxygen reduction activity and stability under acidic

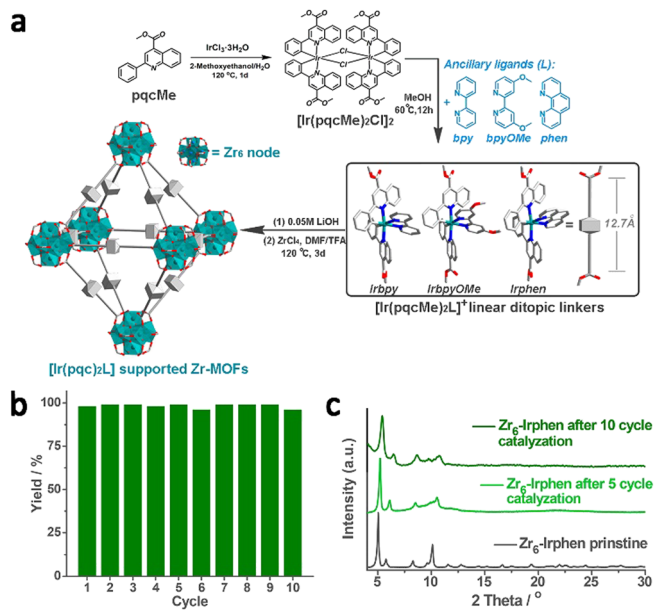

Fig. 10 (a) Illustration of the synthesis process of Ir(III) – Zr MOFs. (b) Cyclic tests of Zr_6–Irphen for photooxidation of methylphenyl sulfide. Reproduced from ref. 166 with permission from the American Chemical Society, copyright 2019.

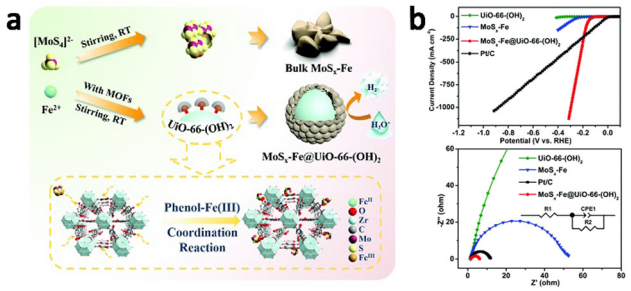

Fig. 12 (a) Schematic diagram of the synthesis of catalysts. (b) Linear cyclic voltammetry curves and Nyquist plots of samples. Reproduced from ref. 173 with permission from the Royal Society of Chemistry, copyright 2020.

and alkaline conditions. In 0.1 M KOH, the half wave potential was as follows: Fe_{SA}–N–C (0.891 V) > Fe_{NP}–N–C (0.889 V) > Pt/C (0.848 V) > Fe_0–N–C (0.795 V) and the order of kinetic current density (J_k) at 0.85 V was Fe_{SA}–N–C (23.27 mA cm^{-2}) > Fe_{NP}–N–C (18.43 mA cm^{-2}) > Pt/C (5.61 mA cm^{-2}) > Fe_0–N–C (0.98 mA cm^{-2}), which exhibited the best oxygen reduction behavior of Fe_{SA}–N–C. Furthermore, we explored their properties in 0.1 M $HClO_4$, and found that Fe_{SA}–N–C still showed excellent ORR activity under acidic conditions ($E_{1/2}$ = 0.776 V). These excellent performances could be attributed to the graded porous structure of Fe_{SA}–N–C, the significant active site of monatomic Fe and the high electrical conductivity.[174] We also synthesized a series of M_1–N–C (M = Fe, Co, Ni and Cu) based on MTV-MOFs, which can be efficiently used for electrocatalytic CO_2 reduction. Among all the tested samples, Ni_1–N–C had the highest CO Faraday efficiency (FE = 96.8%), and the turnover frequency (TOF) was as high as 11 315 h^{-1} in pure CO_2. Even at low concentrations of CO_2, Ni_1–N–C still maintained high selectivity. Fig. 13 expressed the CO generation process of the CO_2RR, in which the formation of *COOH was considered to be the decisive factor in the system. The *COOH formation energy barrier and CO desorption energy barrier of Ni_1–N–C were both lower than others, which fully explained the excellent CO_2 reduction activity of Ni_1–N–C. In addition, due to the inevitable HER, the more regular the limiting potential difference between CO_2RR and HER ($U_L(CO_2)$–$U_L(H_2)$), the higher the

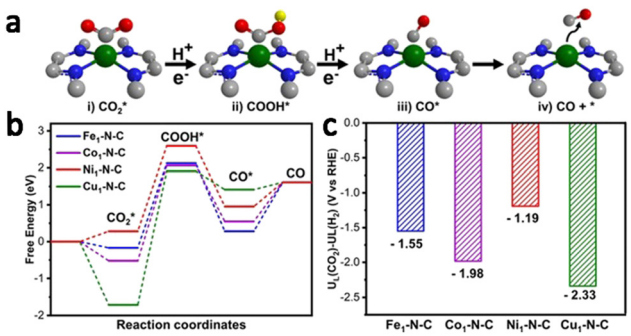

Fig. 13 Calculations: (a) reaction process. (b) Free energy of CO_2 reduction. (c) The $U_L(CO_2)$–$U_L(H_2)$ for all catalysts. Reproduced from ref. 175 with permission from the Wiley-VCH, copyright 2020.

CO_2RR selectivity.[175] Later, we reported a dual protection strategy, which effectively constricted Fe aggregation during pyrolysis with the assistance of SiO_2 (FeN_4/SiO_2), thus making the loading of Fe as high as 3.46 wt%. Fe_{SA}–N–C gave an outstanding oxygen reduction performance under both acidic and alkaline conditions.[176]

Jin *et al.* fabricated Zr-MOF composed of redox-reversible tetrathiafulvalene (TTF) derivatives and Zr_6 nanoclusters to efficiently electro-catalyze the conversion of nitrate to NH_3, in which ultrafine noble metal nanodots (NDs) could be uniformly grown on MOFs to form M-NDs/Zr-MOF (M = Pd, Ag, or Au). Based on the mass transfer process caused by the good conductivity of highly porous Zr-MOF and the powerful interactions between MOF and the active substance, Pd-NDs/Zr MOF showed the superior electrocatalytic activity (NH_3 yield rate ~287.31 mmol h^{-1} $g_{cat.}^{-1}$) among all the tested catalysts.[177]

5 Conclusion and prospects

The past two decades have witnessed a tremendous development of Zr- and Ti-MOFs. Thousands of Zr- and Ti-MOF materials were synthesized and characterized, however, there are still some important aspects of concern:

(1) The structures of pristine MOFs can be viewed as the permutation and combination of metal ions/clusters, organic linkers and guest molecular species. It is quite intriguing that the abundant structures of Zr- and Ti-MOFs give rise to multiple unique MOFs based on the same molecular building blocks, however, obtaining the pure phase is a challenge in a one-pot reaction. Thus, how to control the interpenetration when using enlarged linkers and an engineered pore environment needs to be further optimized.

(2) In terms of the synthesis of Zr- and Ti-MOFs, conventional hydrothermal/solvothermal synthesis is still the dominant synthesis method. More attention should be paid to some emerging techniques, including electrochemistry, mechanochemistry, microwave, ultrasonic radiation and room temperature stirring. From the perspective of green chemistry, environmentally benign solvents should be considered such as water and ethanol, instead of organic solvents. Thus, how to control the hydrolysis of Zr and Ti precursors is particularly important.

(3) The chemical and thermal stabilities of Zr- and Ti-MOFs have also been improved to a great extent, but the mechanical stability is not satisfactory, which limits processing and shaping of MOFs in industrial applications.

(4) Experimental and theoretical studies on the mechanism of Zr- and Ti-MOF assembly are urgently needed.

(5) In order to lower costs and maximize the synergistic performance of component materials, Zr- and Ti-MOF-based composites and membranes should be well investigated in the future.

Author contributions

L. Zhang and H.-L. Jiang conceived and directed the project. J. Li and L. Zhang wrote the manuscript; Y. Meng, J. Huang and

L. Li were responsible for researching and organizing the literature on Zr- and Ti-based metal organic frameworks. L. Zhang, L. Li and H.-L. Jiang were responsible for the format modification and inspection of the paper.

Conflicts of interest

There are no conflicts to declare.

Acknowledgements

This work was financially supported by the National Key Research and Development Program of China (2021YFA1500400), the National Natural Science Foundation of China (22161142001 and U22A20401), Ningbo Natural Science Foundation (202003N4066) and the Natural Science Basic Research Program of Shaanxi (2023-JC-YB-088).

References

1 H. Furukawa, K. E. Cordova, M. O'Keeffe and O. M. Yaghi, *Science*, 2013, **341**, 1230444.
2 S. Kitagawa, R. Kitaura and S. Noro, *Angew. Chem., Int. Ed.*, 2004, **43**, 2334–2375.
3 A. J. Howarth, Y. Liu, P. Li, Z. Li, T. C. Wang, J. T. Hupp and O. K. Farha, *Nat. Rev. Mater.*, 2016, **1**, 15018.
4 Z. Chen, S. L. Hanna, L. R. Redfern, D. Alezi, T. Islamoglu and O. K. Farha, *Coordin. Chem. Rev.*, 2019, **386**, 32–49.
5 X. Zhang, W. Fan, M. Fu, W. Jiang, K. Lu, Y. Wang and D. Sun, *Chem. Commun.*, 2020, **56**, 10513–10516.
6 Y. Wang, M. Fu, S. Zhou, H. Liu, X. Wang, W. Fan, Z. Liu, Z. Wang, D. Li, H. Hao, X. Lu, S. Hu and D. Sun, *Chem*, 2022, **8**, 3263–3274.
7 W. Fan, S. Yuan, W. Wang, L. Feng, X. Liu, X. Zhang, X. Wang, Z. Kang, F. Dai, D. Yuan, D. Sun and H.-C. Zhou, *J. Am. Chem. Soc.*, 2020, **142**, 8728–8737.
8 M. Ding and H.-L. Jiang, *CCS Chem.*, 2021, **3**, 2740–2748.
9 J. H. Cavka, S. Jakobsen, U. Olsbye, N. Guillou, C. Lamberti, S. Bordiga and K. P. Lillerud, *J. Am. Chem. Soc.*, 2008, **130**, 13850–13851.
10 M. Dan-Hardi, C. Serre, T. Frot, L. Rozes, G. Maurin, C. Sanchez and G. Ferey, *J. Am. Chem. Soc.*, 2009, **131**, 10857–10859.
11 T. Devic and C. Serre, *Chem. Soc. Rev.*, 2014, **43**, 6097–6115.
12 L. Feng, G. S. Day, K.-Y. Wang, S. Yuan and H.-C. Zhou, *Chem*, 2020, **6**, 2902–2923.
13 J. I. Choi, H. Chun and M. S. Lah, *J. Am. Chem. Soc.*, 2018, **140**, 10915–10920.
14 E. M. El-Sayed, Y. D. Yuan, D. Zhao and D. Yuan, *Acc. Chem. Res.*, 2022, **55**, 1546–1560.
15 P. Ji, K. Manna, Z. Lin, X. Feng, A. Urban, Y. Song and W. Lin, *J. Am. Chem. Soc.*, 2017, **139**, 7004–7011.
16 G. Kickelbick, D. Holzinger, C. Brick, G. Trimmel and E. Moons, *Chem. Mater.*, 2002, **14**, 4382–4389.
17 H. Assi, G. Mouchaham, N. Steunou, T. Devic and C. Serre, *Chem. Soc. Rev.*, 2017, **46**, 3431–3452.
18 Y. Bai, Y. Dou, L. H. Xie, W. Rutledge, J. R. Li and H.-C. Zhou, *Chem. Soc. Rev.*, 2016, **45**, 2327–2367.
19 L. Feng, J. Pang, P. She, J. L. Li, J. S. Qin, D. Y. Du and H.-C. Zhou, *Adv. Mater.*, 2020, **32**, e2004414.
20 J. Lippke, B. Brosent, T. von Zons, E. Virmani, S. Lilienthal, T. Preusse, M. Hulsmann, A. M. Schneider, S. Wuttke, P. Behrens and A. Godt, *Inorg. Chem.*, 2017, **56**, 748–761.
21 A. Schaate, P. Roy, T. Preusse, S. J. Lohmeier, A. Godt and P. Behrens, *Chem. – Eur. J.*, 2011, **17**, 9320–9325.
22 L. Feng, S. Yuan, J.-S. Qin, Y. Wang, A. Kirchon, D. Qiu, L. Cheng, S. T. Madrahimov and H.-C. Zhou, *Matter*, 2019, **1**, 156–167.
23 S. Yuan, L. Huang, Z. Huang, D. Sun, J. S. Qin, L. Feng, J. Li, X. Zou, T. Cagin and H.-C. Zhou, *J. Am. Chem. Soc.*, 2020, **142**, 4732–4738.
24 V. Bon, V. Senkovskyy, I. Senkovska and S. Kaskel, *Chem. Commun.*, 2012, **48**, 8407–8409.
25 V. Bon, I. Senkovska, I. A. Baburin and S. Kaskel, *Cryst. Growth Des.*, 2013, **13**, 1231–1237.
26 S. Yuan, Y. P. Chen, J. S. Qin, W. Lu, L. Zou, Q. Zhang, X. Wang, X. Sun and H.-C. Zhou, *J. Am. Chem. Soc.*, 2016, **138**, 8912–8919.
27 S. Yuan, W. Lu, Y. P. Chen, Q. Zhang, T. F. Liu, D. Feng, X. Wang, J. Qin and H.-C. Zhou, *J. Am. Chem. Soc.*, 2015, **137**, 3177–3180.
28 S. Krause, V. Bon, U. Stoeck, I. Senkovska, D. M. Tobbens, D. Wallacher and S. Kaskel, *Angew. Chem., Int. Ed.*, 2017, **56**, 10676–10680.
29 P. Y. Du, W. P. Lustig, S. J. Teat, W. Gu, X. Liu and J. Li, *Chem. Commun.*, 2018, **54**, 8088–8091.
30 B. Lu, Y. Chen, P. Li, B. Wang, K. Mullen and M. Yin, *Nat. Commun.*, 2019, **10**, 767.
31 V. Bon, I. Senkovska, M. S. Weiss and S. Kaskel, *CrystEngComm*, 2013, **15**, 9572.
32 V. Guillerm and D. Maspoch, *J. Am. Chem. Soc.*, 2019, **141**, 16517–16538.
33 H. Furukawa, F. Gandara, Y. B. Zhang, J. Jiang, W. L. Queen, M. R. Hudson and O. M. Yaghi, *J. Am. Chem. Soc.*, 2014, **136**, 4369–4381.
34 D. Feng, K. Wang, J. Su, T. F. Liu, J. Park, Z. Wei, M. Bosch, A. Yakovenko, X. Zou and H.-C. Zhou, *Angew. Chem., Int. Ed.*, 2015, **54**, 149–154.
35 R. Wang, Z. Wang, Y. Xu, F. Dai, L. Zhang and D. Sun, *Inorg. Chem.*, 2014, **53**, 7086–7088.
36 L. Cao, T. Wang and C. Wang, *Chin. J. Chem.*, 2018, **36**, 754–764.
37 B. Wang, X. L. Lv, D. Feng, L. H. Xie, J. Zhang, M. Li, Y. Xie, J. R. Li and H.-C. Zhou, *J. Am. Chem. Soc.*, 2016, **138**, 6204–6216.
38 S. Lee, H. B. Burgi, S. A. Alshmimri and O. M. Yaghi, *J. Am. Chem. Soc.*, 2018, **140**, 8958–8964.
39 T. F. Liu, N. A. Vermeulen, A. J. Howarth, P. Li, A. A. Sarjeant, J. T. Hupp and O. K. Farha, *Eur. J. Inorg. Chem.*, 2016, 4349–4352.
40 T. He, Y. Z. Zhang, X. J. Kong, J. Yu, X. L. Lv, Y. Wu, Z. J. Guo and J. R. Li, *ACS Appl. Mater. Interfaces*, 2018, **10**, 16650–16659.
41 Y. Zhao, S. Qi, Z. Niu, Y. Peng, C. Shan, G. Verma, L. Wojtas, Z. Zhang, B. Zhang, Y. Feng, Y. S. Chen and S. Ma, *J. Am. Chem. Soc.*, 2019, **141**, 14443–14450.
42 V. Guillerm, L. Weselinski, Y. Belmabkhout, A. J. Cairns, V. D'Elia, L. Wojtas, K. Adil and M. Eddaoudi, *Nat. Chem.*, 2014, **6**, 673–680.
43 G. Jin, D. Sensharma, N. Zhu, S. Vaesen and W. Schmitt, *Dalton Trans.*, 2019, **48**, 15487–15492.
44 B. Guo, F. Li, C. Wang, L. Zhang and D. Sun, *J. Mater. Chem. A*, 2019, **7**, 13173–13179.
45 W. Morris, B. Volosskiy, S. Demir, F. Gandara, P. L. McGrier, H. Furukawa, D. Cascio, J. F. Stoddart and O. M. Yaghi, *Inorg. Chem.*, 2012, **51**, 6443–6445.
46 D. Feng, Z. Y. Gu, J. R. Li, H. L. Jiang, Z. Wei and H.-C. Zhou, *Angew. Chem., Int. Ed.*, 2012, **51**, 10307–10310.
47 T. E. Webber, W. G. Liu, S. P. Desai, C. C. Lu, D. G. Truhlar and R. L. Penn, *ACS Appl. Mater. Interfaces*, 2017, **9**, 39342–39346.
48 J. E. Mondloch, W. Bury, D. Fairen-Jimenez, S. Kwon, E. J. DeMarco, M. H. Weston, A. A. Sarjeant, S. T. Nguyen, P. C. Stair, R. Q. Snurr, O. K. Farha and J. T. Hupp, *J. Am. Chem. Soc.*, 2013, **135**, 10294–10297.
49 Y. Chen, T. Hoang and S. Ma, *Inorg. Chem.*, 2012, **51**, 12600–12602.
50 H. L. Jiang, D. Feng, K. Wang, Z. Y. Gu, Z. Wei, Y. P. Chen and H.-C. Zhou, *J. Am. Chem. Soc.*, 2013, **135**, 13934–13938.
51 C.-W. Kung, T. C. Wang, J. E. Mondloch, D. Fairen-Jimenez, D. M. Gardner, W. Bury, J. M. Klingsporn, J. C. Barnes, R. Van Duyne, J. F. Stoddart, M. R. Wasielewski, O. K. Farha and J. T. Hupp, *Chem. Mater.*, 2013, **25**, 5012–5017.
52 S. J. Garibay, I. Iordanov, T. Islamoglu, J. B. DeCoste and O. K. Farha, *CrystEngComm*, 2018, **20**, 7066–7070.
53 P. Deria, D. A. Gomez-Gualdron, I. Hod, R. Q. Snurr, J. T. Hupp and O. K. Farha, *J. Am. Chem. Soc.*, 2016, **138**, 14449–14457.
54 M. Zhang, Y. P. Chen, M. Bosch, T. Gentle, 3rd, K. Wang, D. Feng, Z. U. Wang and H.-C. Zhou, *Angew. Chem., Int. Ed.*, 2014, **53**, 815–818.
55 D. Feng, Z. Y. Gu, Y. P. Chen, J. Park, Z. Wei, Y. Sun, M. Bosch, S. Yuan and H.-C. Zhou, *J. Am. Chem. Soc.*, 2014, **136**, 17714–17717.
56 D. Feng, W.-C. Chung, Z. Wei, Z.-Y. Gu, H.-L. Jiang, Y.-P. Chen, D. J. Darensbourg and H.-C. Zhou, *J. Am. Chem. Soc.*, 2013, **135**, 17105–17110.

57 J. Ma, L. D. Tran and A. J. Matzger, *Cryst. Growth Des.*, 2016, **16**, 4148–4153.
58 J. Pang, S. Yuan, J. Qin, C. Liu, C. Lollar, M. Wu, D. Yuan, H.-C. Zhou and M. Hong, *J. Am. Chem. Soc.*, 2017, **139**, 16939–16945.
59 X. L. Lv, S. Yuan, L. H. Xie, H. F. Darke, Y. Chen, T. He, C. Dong, B. Wang, Y. Z. Zhang, J. R. Li and H.-C. Zhou, *J. Am. Chem. Soc.*, 2019, **141**, 10283–10293.
60 G. Cai, P. Yan, L. Zhang, H.-C. Zhou and H.-L. Jiang, *Chem. Rev.*, 2021, **121**, 12278–12326.
61 L. Yang, P. Cai, L. Zhang, X. Xu, A. A. Yakovenko, Q. Wang, J. Pang, S. Yuan, X. Zou, N. Huang, Z. Huang and H.-C. Zhou, *J. Am. Chem. Soc.*, 2021, **143**, 12129–12137.
62 W. Gong, X. Chen, H. Jiang, D. Chu, Y. Cui and Y. Liu, *J. Am. Chem. Soc.*, 2019, **141**, 7498–7508.
63 H. Jiang, W. Zhang, X. Kang, Z. Cao, X. Chen, Y. Liu and Y. Cui, *J. Am. Chem. Soc.*, 2020, **142**, 9642–9652.
64 Y. Zhang, X. Zhang, J. Lyu, K. I. Otake, X. Wang, L. R. Redfern, C. D. Malliakas, Z. Li, T. Islamoglu, B. Wang and O. K. Farha, *J. Am. Chem. Soc.*, 2018, **140**, 11179–11183.
65 P. T. K. Nguyen, H. T. D. Nguyen, H. N. Nguyen, C. A. Trickett, Q. T. Ton, E. Gutierrez-Puebla, M. A. Monge, K. E. Cordova and F. Gandara, *ACS Appl. Mater. Interfaces*, 2018, **10**, 733–744.
66 Z. Duan, Y. Li, X. Xiao, X. Huang, X. Li, Y. Li, C. Zhang, H. Zhang, L. Li, Z. Lin, Y. Zhao and W. Huang, *ACS Appl. Mater. Interfaces*, 2020, **12**, 18715–18722.
67 S. Jia, X. Xiao, Q. Li, Y. Li, Z. Duan, Y. Li, X. Li, Z. Lin, Y. Zhao and W. Huang, *Inorg. Chem.*, 2019, **58**, 12748–12755.
68 Y. Li, X. Li, S. Jia, C. Zhang, Y. Luo, Z. Lin, Y. Zhao and W. Huang, *Inorg. Chem.*, 2021, **60**, 12129–12135.
69 C. Zhang, Y. Luo, Y. Li, B. Zhao, Z. Yang, X. Li, J. Duan, Y. Zhao, Z. Lin and W. Huang, *Cryst. Growth Des.*, 2022, **22**, 6384–6389.
70 A. Cadiau, L. S. Xie, N. Kolobov, A. Shkurenko, M. Qureshi, M. R. Tchalala, S. S. Park, A. Bavykina, M. Eddaoudi, M. Dincă, C. H. Hendon and J. Gascon, *Chem. Mater.*, 2019, **32**, 97–104.
71 Y. Wang, L. Feng, K. Zhang, K. Y. Wang, W. Fan, X. Wang, B. Guo, F. Dai, L. Zhang, D. Sun and H.-C. Zhou, *Adv. Sci.*, 2019, **6**, 1901855.
72 D. Alezi, I. Spanopoulos, C. Tsangarakis, A. Shkurenko, K. Adil, Y. Belmabkhout, M. O'Keeffe, M. Eddaoudi and P. N. Trikalitis, *J. Am. Chem. Soc.*, 2016, **138**, 12767–12770.
73 J. S. Qin, S. Yuan, L. Zhang, B. Li, D. Y. Du, N. Huang, W. Guan, H. F. Drake, J. Pang, Y. Q. Lan, A. Alsalme and H.-C. Zhou, *J. Am. Chem. Soc.*, 2019, **141**, 2054–2060.
74 Z. Chen, K. O. Kirlikovali, P. Li and O. K. Farha, *Acc. Chem. Res.*, 2022, **55**, 579–591.
75 X. Chen, X. Peng, L. Jiang, X. Yuan, H. Yu, H. Wang, J. Zhang and Q. Xia, *Chem. Eng. J.*, 2020, **395**, 125080.
76 S. Yuan, J. S. Qin, C. T. Lollar and H.-C. Zhou, *ACS Cent. Sci.*, 2018, **4**, 440–450.
77 C. Zlotea, D. Phanon, M. Mazaj, D. Heurtaux, V. Guillerm, C. Serre, P. Horcajada, T. Devic, E. Magnier, F. Cuevas, G. Ferey, P. L. Llewellyn and M. Latroche, *Dalton Trans.*, 2011, **40**, 4879–4881.
78 Y. Fu, D. Sun, Y. Chen, R. Huang, Z. Ding, X. Fu and Z. Li, *Angew. Chem., Int. Ed.*, 2012, **51**, 3364–3367.
79 B. Bueken, F. Vermoortele, D. E. Vanpoucke, H. Reinsch, C. C. Tsou, P. Valvekens, T. De Baerdemaeker, R. Ameloot, C. E. Kirschhock, V. Van Speybroeck, J. M. Mayer and D. De Vos, *Angew. Chem., Int. Ed.*, 2015, **54**, 13912–13917.
80 J. A. Mason, L. E. Darago, W. W. Lukens, Jr. and J. R. Long, *Inorg. Chem.*, 2015, **54**, 10096–10104.
81 Y. Song, Z. Li, Y. Zhu, X. Feng, J. S. Chen, M. Kaufmann, C. Wang and W. Lin, *J. Am. Chem. Soc.*, 2019, **141**, 12219–12223.
82 X. Feng, Y. Song, J. S. Chen, Z. Li, E. Y. Chen, M. Kaufmann, C. Wang and W. Lin, *Chem. Sci.*, 2019, **10**, 2193–2198.
83 H. L. Nguyen, F. Gandara, H. Furukawa, T. L. Doan, K. E. Cordova and O. M. Yaghi, *J. Am. Chem. Soc.*, 2016, **138**, 4330–4333.
84 H. L. Nguyen, T. T. Vu, D. Le, T. L. H. Doan, V. Q. Nguyen and N. T. S. Phan, *ACS Catal.*, 2016, **7**, 338–342.
85 H. L. Nguyen, *New J. Chem.*, 2017, **41**, 14030–14043.
86 L. Zou, D. Feng, T. F. Liu, Y. P. Chen, S. Yuan, K. Wang, X. Wang, S. Fordham and H.-C. Zhou, *Chem. Sci.*, 2016, **7**, 1063–1069.
87 J. Castells-Gil, N. M. Padial, N. Almora-Barrios, I. da Silva, D. Mateo, J. Albero, H. Garcia and C. Marti-Gastaldo, *Chem. Sci.*, 2019, **10**, 4313–4321.
88 C. Li, H. Xu, J. Gao, W. Du, L. Shangguan, X. Zhang, R.-B. Lin, H. Wu, W. Zhou, X. Liu, J. Yao and B. Chen, *J. Mater. Chem. A*, 2019, **7**, 11928–11933.
89 S. Wang, H. Reinsch, N. Heymans, M. Wahiduzzaman, C. Martineau-Corcos, G. De Weireld, G. Maurin and C. Serre, *Matter*, 2020, **2**, 440–450.
90 S. Wang, M. Cabrero-Antonino, S. Navalón, C.-C. Cao, A. Tissot, I. Dovgaliuk, J. Marrot, C. Martineau-Corcos, L. Yu, H. Wang, W. Shepard, H. García and C. Serre, *Chem*, 2020, **6**, 3409–3427.
91 S. Yuan, T. F. Liu, D. Feng, J. Tian, K. Wang, J. Qin, Q. Zhang, Y. P. Chen, M. Bosch, L. Zou, S. J. Teat, S. J. Dalgarno and H.-C. Zhou, *Chem. Sci.*, 2015, **6**, 3926–3930.
92 Y. Keum, S. Park, Y. P. Chen and J. Park, *Angew. Chem., Int. Ed.*, 2018, **57**, 14852–14856.
93 G. Lan, K. Ni, S. S. Veroneau, X. Feng, G. T. Nash, T. Luo, Z. Xu and W. Lin, *J. Am. Chem. Soc.*, 2019, **141**, 4204–4208.
94 A. Cadiau, N. Kolobov, S. Srinivasan, M. G. Goesten, H. Haspel, A. V. Bavykina, M. R. Tchalala, P. Maity, A. Goryachev, A. S. Poryvaev, M. Eddaoudi, M. V. Fedin, O. F. Mohammed and J. Gascon, *Angew. Chem., Int. Ed.*, 2020, **59**, 13468–13472.
95 C. Wang, C. Liu, X. He and Z. M. Sun, *Chem. Commun.*, 2017, **53**, 11670–11673.
96 M. Kim, J. F. Cahill, H. Fei, K. A. Prather and S. M. Cohen, *J. Am. Chem. Soc.*, 2012, **134**, 18082–18088.
97 M. S. Denny, Jr., L. R. Parent, J. P. Patterson, S. K. Meena, H. Pham, P. Abellan, Q. M. Ramasse, F. Paesani, N. C. Gianneschi and S. M. Cohen, *J. Am. Chem. Soc.*, 2018, **140**, 1348–1357.
98 R. Navarro Amador, M. Carboni and D. Meyer, *RSC Adv.*, 2017, **7**, 195–200.
99 D. Sun, W. Liu, M. Qiu, Y. Zhang and Z. Li, *Chem. Commun.*, 2015, **51**, 2056–2059.
100 Y. Lee, S. Kim, J. K. Kang and S. M. Cohen, *Chem. Commun.*, 2015, **51**, 5735–5738.
101 J. Tu, X. Zeng, F. Xu, X. Wu, Y. Tian, X. Hou and Z. Long, *Chem. Commun.*, 2017, **53**, 3361–3364.
102 M. Chen, Z. Long, R. Dong, L. Wang, J. Zhang, S. Li, X. Zhao, X. Hou, H. Shao and X. Jiang, *Small*, 2020, **16**, e1906240.
103 J. G. Santaclara, A. I. Olivos-Suarez, A. Gonzalez-Nelson, D. Osadchii, M. A. Nasalevich, M. A. van der Veen, F. Kapteijn, A. M. Sheveleva, S. L. Veber, M. V. Fedin, A. T. Murray, C. H. Hendon, A. Walsh and J. Gascon, *Chem. Mater.*, 2017, **29**, 8963–8967.
104 Z. Huang, D. Liu, J. Camacho-Bunquin, G. Zhang, D. Yang, J. M. López-Encarnación, Y. Xu, M. S. Ferrandon, J. Niklas, O. G. Poluektov, J. Jellinek, A. Lei, E. E. Bunel and M. Delferro, *Organometallics*, 2017, **36**, 3921–3930.
105 I. S. Kim, J. Borycz, A. E. Platero-Prats, S. Tussupbayev, T. C. Wang, O. K. Farha, J. T. Hupp, L. Gagliardi, K. W. Chapman, C. J. Cramer and A. B. F. Martinson, *Chem. Mater.*, 2015, **27**, 4772–4778.
106 R. C. Klet, T. C. Wang, L. E. Fernandez, D. G. Truhlar, J. T. Hupp and O. K. Farha, *Chem. Mater.*, 2016, **28**, 1213–1219.
107 C.-W. Kung, J. E. Mondloch, T. C. Wang, W. Bury, W. Hoffeditz, B. M. Klahr, R. C. Klet, M. J. Pellin, O. K. Farha and J. T. Hupp, *ACS Appl. Mater. Interfaces*, 2015, **7**, 28223–28230.
108 Z. Li, A. W. Peters, V. Bernales, M. A. Ortuno, N. M. Schweitzer, M. R. DeStefano, L. C. Gallington, A. E. Platero-Prats, K. W. Chapman, C. J. Cramer, L. Gagliardi, J. T. Hupp and O. K. Farha, *ACS Cent. Sci.*, 2017, **3**, 31–38.
109 Z. Li, A. W. Peters, A. E. Platero-Prats, J. Liu, C. W. Kung, H. Noh, M. R. DeStefano, N. M. Schweitzer, K. W. Chapman, J. T. Hupp and O. K. Farha, *J. Am. Chem. Soc.*, 2017, **139**, 15251–15258.
110 S. Yuan, Y. P. Chen, J. Qin, W. Lu, X. Wang, Q. Zhang, M. Bosch, T. F. Liu, X. Lian and H.-C. Zhou, *Angew. Chem., Int. Ed.*, 2015, **127**, 14909–14913.
111 X. Wang, K. Ma, T. Goh, M. R. Mian, H. Xie, H. Mao, J. Duan, K. O. Kirlikovali, A. Stone, D. Ray, M. R. Wasielewski, L. Gagliardi and O. K. Farha, *J. Am. Chem. Soc.*, 2022, **144**, 12192–12201.
112 S. Yuan, J. S. Qin, H. Q. Xu, J. Su, D. Rossi, Y. Chen, L. Zhang, C. Lollar, Q. Wang, H.-L. Jiang, D. H. Son, H. Xu, Z. Huang, X. Zou and H.-C. Zhou, *ACS Cent. Sci.*, 2018, **4**, 105–111.
113 A. Helal, Z. H. Yamani, K. E. Cordova and O. M. Yaghi, *Natl. Sci. Rev.*, 2017, **4**, 296–298.
114 H. Deng, C. J. Doonan, H. Furukawa, R. B. Ferreira, J. Towne, C. B. Knobler, B. Wang and O. M. Yaghi, *Science*, 2010, **327**, 846–850.

115 L. Liu, K. Konstas, M. R. Hill and S. G. Telfer, *J. Am. Chem. Soc.*, 2013, **135**, 17731–17734.
116 L. Liu and S. G. Telfer, *J. Am. Chem. Soc.*, 2015, **137**, 3901–3909.
117 J. Cornelio, T. Y. Zhou, A. Alkas and S. G. Telfer, *J. Am. Chem. Soc.*, 2018, **140**, 15470–15476.
118 M. Lammert, C. Glissmann and N. Stock, *Dalton Trans.*, 2017, **46**, 2425–2429.
119 A. Dutta, Y. Pan, J.-Q. Liu and A. Kumar, *Coordin. Chem. Rev.*, 2021, **445**, 214074.
120 S. Kitagawa, *Acc. Chem. Res.*, 2017, **50**, 514–516.
121 Y. Sun, L. Sun, D. Feng and H.-C. Zhou, *Angew. Chem., Int. Ed.*, 2016, **55**, 6471–6475.
122 Y. C. Qiu, S. Yuan, X. X. Li, D. Y. Du, C. Wang, J. S. Qin, H. F. Drake, Y. Q. Lan, L. Jiang and H.-C. Zhou, *J. Am. Chem. Soc.*, 2019, **141**, 13841–13848.
123 J. Pang, S. Yuan, J. Qin, M. Wu, C. T. Lollar, J. Li, N. Huang, B. Li, P. Zhang and H.-C. Zhou, *J. Am. Chem. Soc.*, 2018, **140**, 12328–12332.
124 X. Zhang, B. L. Frey, Y. S. Chen and J. Zhang, *J. Am. Chem. Soc.*, 2018, **140**, 7710–7715.
125 L. J. Wang, H. Deng, H. Furukawa, F. Gandara, K. E. Cordova, D. Peri and O. M. Yaghi, *Inorg. Chem.*, 2014, **53**, 5881–5883.
126 S. Abednatanzi, P. Gohari Derakhshandeh, H. Depauw, F. X. Coudert, H. Vrielinck, P. Van Der Voort and K. Leus, *Chem. Soc. Rev.*, 2019, **48**, 2535–2565.
127 S. Yuan, J. Peng, Y. Zhang and Y. Shao-Horn, *J. Phys. Chem. C*, 2019, **123**, 28266–28274.
128 L. Zhang, S. Yuan, L. Feng, B. Guo, J. S. Qin, B. Xu, C. Lollar, D. Sun and H-C. Zhou, *Angew. Chem., Int. Ed.*, 2018, **57**, 5095–5099.
129 F. Saraci, V. Quezada-Novoa, P. R. Donnarumma and A. J. Howarth, *Chem. Soc. Rev.*, 2020, **49**, 7949–7977.
130 Z. Hu, Y. Wang and D. Zhao, *Chem. Soc. Rev.*, 2021, **50**, 4629–4683.
131 F. Nouar, M. I. Breeze, B. C. Campo, A. Vimont, G. Clet, M. Daturi, T. Devic, R. I. Walton and C. Serre, *Chem. Commun.*, 2015, **51**, 14458–14461.
132 A. M. Ebrahim, B. Levasseur and T. J. Bandosz, *Langmuir*, 2013, **29**, 168–174.
133 M. Lammert, M. T. Wharmby, S. Smolders, B. Bueken, A. Lieb, K. A. Lomachenko, D. D. Vos and N. Stock, *Chem. Commun.*, 2015, **51**, 12578–12581.
134 K. A. Lomachenko, J. Jacobsen, A. L. Bugaev, C. Atzori, F. Bonino, S. Bordiga, N. Stock and C. Lamberti, *J. Am. Chem. Soc.*, 2018, **140**, 17379–17383.
135 S. Yuan, J. S. Qin, J. Li, L. Huang, L. Feng, Y. Fang, C. Lollar, J. Pang, L. Zhang, D. Sun, A. Alsalme, T. Cagin and H.-C. Zhou, *Nat. Commun.*, 2018, **9**, 808.
136 J. E. Mondloch, M. J. Katz, W. C. Isley, 3rd, P. Ghosh, P. Liao, W. Bury, G. W. Wagner, M. G. Hall, J. B. DeCoste, G. W. Peterson, R. Q. Snurr, C. J. Cramer, J. T. Hupp and O. K. Farha, *Nat. Mater.*, 2015, **14**, 512–516.
137 A. M. Abdel-Mageed, B. Rungtaweevoranit, M. Parlinska-Wojtan, X. Pei, O. M. Yaghi and R. J. Behm, *J. Am. Chem. Soc.*, 2019, **141**, 5201–5210.
138 S. H. Liu Bo, A. Tomoki and X. Qiang, *J. Am. Chem. Soc.*, 2008, **130**, 5390–5391.
139 G. Huang, L. Yang, X. Ma, J. Jiang, S. H. Yu and H.-L. Jiang, *Chem. – Eur. J.*, 2016, **22**, 3470–3477.
140 L. Jiao, W. Yang, G. Wan, R. Zhang, X. Zheng, H. Zhou, S. H. Yu and H.-L. Jiang, *Angew. Chem., Int. Ed.*, 2020, **59**, 20589–20595.
141 J. Liang, Y. Q. Xie, Q. Wu, X. Y. Wang, T. T. Liu, H. F. Li, Y. B. Huang and R. Cao, *Inorg. Chem.*, 2018, **57**, 2584–2593.
142 J. Lyu, X. Zhang, K. I. Otake, X. Wang, P. Li, Z. Li, Z. Chen, Y. Zhang, M. C. Wasson, Y. Yang, P. Bai, X. Guo, T. Islamoglu and O. K. Farha, *Chem. Sci.*, 2019, **10**, 1186–1192.
143 L. Zhang, S. Yuan, W. Fan, J. Pang, F. Li, B. Guo, P. Zhang, D. Sun and H.-C. Zhou, *ACS Appl. Mater. Interfaces*, 2019, **11**, 22390–22397.
144 D. Chen, W. Yang, L. Jiao, L. Li, S. H. Yu and H.-L. Jiang, *Adv. Mater.*, 2020, **32**, e2000041.
145 A. H. Valekar, M. Lee, J. W. Yoon, J. Kwak, D.-Y. Hong, K.-R. Oh, G.-Y. Cha, Y.-U. Kwon, J. Jung, J.-S. Chang and Y. K. Hwang, *ACS Catal.*, 2020, **10**, 3720–3732.
146 Z. Chen, P. Li, X. Wang, K. I. Otake, X. Zhang, L. Robison, A. Atilgan, T. Islamoglu, M. G. Hall, G. W. Peterson, J. F. Stoddart and O. K. Farha, *J. Am. Chem. Soc.*, 2019, **141**, 12229–12235.
147 K. Ma, T. Islamoglu, Z. Chen, P. Li, M. C. Wasson, Y. Chen, Y. Wang, G. W. Peterson, J. H. Xin and O. K. Farha, *J. Am. Chem. Soc.*, 2019, **141**, 15626–15633.
148 X. Liu, K. O. Kirlikovali, Z. Chen, K. Ma, K. B. Idrees, R. Cao, X. Zhang, T. Islamoglu, Y. Liu and O. K. Farha, *Chem. Mater.*, 2021, **33**, 1444–1454.
149 K. Kiaei, M. T. Nord, N. C. Chiu and K. C. Stylianou, *ACS Appl. Mater. Interfaces*, 2022, **14**, 19747–19755.
150 Y. Ko, E. J. Bae, S. K. Chitale, C. V. Soares, A. A. Leitão, M.-K. Kim, J.-S. Chang, G. Maurin, S. G. Ryu and U. H. Lee, *ACS Appl. Nano Mater.*, 2022, **5**, 9657–9665.
151 D. Li, S. H. Yu and H.-L. Jiang, *Adv. Mater.*, 2018, **30**, e1707377.
152 H. Liu, C. Xu, D. Li and H.-L. Jiang, *Angew. Chem., Int. Ed.*, 2018, **57**, 5379–5383.
153 Y. Pan, D. Li and H. L. Jiang, *Chem. – Eur. J.*, 2018, **24**, 18403–18407.
154 P. Tian, X. He, L. Zhao, W. Li, W. Fang, H. Chen, F. Zhang, Z. Huang and H. Wang, *Int. J. Hydrogen Energy*, 2019, **44**, 788–800.
155 F. Guo, J. H. Guo, P. Wang, Y. S. Kang, Y. Liu, J. Zhao and W. Y. Sun, *Chem. Sci.*, 2019, **10**, 4834–4838.
156 X. Ma, L. Wang, Q. Zhang and H.-L. Jiang, *Angew. Chem., Int. Ed.*, 2019, **58**, 12175–12179.
157 P. Karthik, A. R. M. Shaheer, A. Vinu and B. Neppolian, *Small*, 2020, **16**, e1902990.
158 K. Sun, M. Liu, J. Pei, D. Li, C. Ding, K. Wu and H.-L. Jiang, *Angew. Chem., Int. Ed.*, 2020, **59**, 22749–22755.
159 J. Sui, H. Liu, S. Hu, K. Sun, G. Wan, H. Zhou, X. Zheng and H.-L. Jiang, *Adv. Mater.*, 2022, **34**, e2109203.
160 C. X. Chen, Y. Y. Xiong, X. Zhong, P. C. Lan, Z. W. Wei, H. Pan, P. Y. Su, Y. Song, Y. F. Chen, A. Nafady, U. Siraj and S. Ma, *Angew. Chem., Int. Ed.*, 2022, **61**, e202114071.
161 M. Xu, D. Li, K. Sun, L. Jiao, C. Xie, C. Ding and H.-L. Jiang, *Angew. Chem., Int. Ed.*, 2021, **60**, 16372–16376.
162 C. Zhang, C. Xie, Y. Gao, X. Tao, C. Ding, F. Fan and H.-L. Jiang, *Angew. Chem., Int. Ed.*, 2022, **61**, e202204108.
163 W. Fan, X. Wang, B. Xu, Y. Wang, D. Liu, M. Zhang, Y. Shang, F. Dai, L. Zhang and D. Sun, *J. Mater. Chem. A*, 2018, **6**, 24486–24495.
164 J. Abdi, M. Yahyanezhad, S. Sakhaie, M. Vossoughi and I. Alemzadeh, *J. Environ. Chem. Eng.*, 2019, **7**, 103096.
165 L. Yang, Y. Wang, J. Yuan, G. Wang, Q. Cao, H. Fei, M. Li, J. Shao, H. Li and J. Lu, *Chem. Eng. J.*, 2022, **446**, 137095.
166 L. Q. Wei and B. H. Ye, *ACS Appl. Mater. Interfaces*, 2019, **11**, 41448–41457.
167 D. Sun and D. P. Kim, *ACS Appl. Mater. Interfaces*, 2020, **12**, 20589–20595.
168 K. Gao, H. Li, Q. Meng, J. Wu and H. Hou, *ACS Appl. Mater. Interfaces*, 2021, **13**, 2779–2787.
169 L. L. Ling, W. Yang, P. Yan, M. Wang and H.-L. Jiang, *Angew. Chem., Int. Ed.*, 2022, **61**, e202116396.
170 E. X. Chen, M. Qiu, Y. F. Zhang, Y. S. Zhu, L. Y. Liu, Y. Y. Sun, X. Bu, J. Zhang and Q. Lin, *Adv. Mater.*, 2018, **30**, 1704388.
171 Y. Sun, D.-F. Lu, Y. Sun, M.-Y. Gao, N. Zheng, C. Gu, F. Wang and J. Zhang, *ACS Mater. Lett.*, 2020, **3**, 64–68.
172 S. Dai, T. Kajiwara, M. Ikeda, I. Romero-Muniz, G. Patriarche, A. E. Platero-Prats, A. Vimont, M. Daturi, A. Tissot, Q. Xu and C. Serre, *Angew. Chem., Int. Ed.*, 2022, **61**, e202211848.
173 L. Zhang, Z. Yan, X. Chen, M. Yu, F. Liu, F. Cheng and J. Chen, *Chem. Commun.*, 2020, **56**, 2763–2766.
174 L. Jiao, G. Wan, R. Zhang, H. Zhou, S. H. Yu and H.-L. Jiang, *Angew. Chem., Int. Ed.*, 2018, **57**, 8525–8529.
175 L. Jiao, W. Yang, G. Wan, R. Zhang, X. Zheng, H. Zhou, S. H. Yu and H.-L. Jiang, *Angew. Chem., Int. Ed.*, 2020, **59**, 20589–20595.
176 L. Jiao, R. Zhang, G. Wan, W. Yang, X. Wan, H. Zhou, J. Shui, S. H. Yu and H.-L. Jiang, *Nat. Commun.*, 2020, **11**, 2831.
177 M. Jiang, J. Su, X. Song, P. Zhang, M. Zhu, L. Qin, Z. Tie, J. L. Zuo and Z. Jin, *Nano Lett.*, 2022, **22**, 2529–2537.